for detecting *T. gondii* quantitatively in clinical specimens [13–16]. However, no previous studies have screened other pathogenic agents that could cause necrotizing retinitis in conjunction with *T. gondii*.

In this study, we attempted to measure the *Toxoplasma* genome in ocular samples of patients with clinically suspected ocular *Toxoplasma* by using a two-step PCR system with specific primers and probes for *T. gondii* DNA amplification (*T. gondii* B1 gene). To screen for the human herpes virus and *T. gondii*, the first step used qualitative multiplex PCR to detect the toxoplasma genome in the ocular sample. In the second step, quantitative real-time PCR was used to measure the genomic DNA of *T. gondii*.

Materials and methods

Subjects

This research followed the tenets of the Declaration of Helsinki, with the study protocol approved by the Institutional Ethics Committee of Tokyo Medical and Dental University. Ocular fluid samples were collected only after each patient had provided written informed consent.

Table 1 summarizes the clinical findings observed for patients with ocular toxoplasmosis at their initial presentation. The first patient group was examined between January 2008 and September 2010 at the Tokyo Medical and Dental University Hospital. This group included 13 consecutive patients clinically suspected of having ocular toxoplasmosis based on the serological test for *T. gondii* (serum anti-Toxo IgG: PHA method) and characteristic ocular manifestations. Of these 13 patients, 10 had active intraocular inflammation, that is, there were anterior chamber cells, vitreous opacity, retinal vasculitis, and fresh retinal exudates (focal retinal necrosis). For the other 3 patients, only inactive ocular toxoplasmosis lesions in the form of old pigmented retinal scars were found. For the PCR assay, we collected intraocular fluids from 13 patients (11 aqueous humor and 2 vitreous fluids).

In the second group, we collected 10 samples (8 aqueous humor and 2 vitreous fluid) from 10 patients with other clinical entities of uveitis. The diagnoses for the subjects included idiopathic uveitis ($n = 7$), acute retinal necrosis ($n = 2$), and cytomegalovirus retinitis ($n = 1$). At the time of sampling, all members of this group had active intraocular inflammation.

In the third group, we collected 20 samples (15 aqueous humor and 5 vitreous fluid) from 20 patients with non-inflammatory diseases. The patient diagnoses included age-related cataract ($n = 15$), primary rhegmatogenous retinal detachments ($n = 1$), idiopathic macular hole ($n = 1$), and idiopathic epiretinal membranes ($n = 3$).

The sampling procedures were performed in accordance with the method reported in our previous studies [17–19]. Briefly, we used surgical microscopy to aseptically collect aliquots of approximately 0.1 ml aqueous humor in a syringe with a 30 G needle. Non-diluted vitreous fluid (approximately 0.5 ml) was collected during the pars plana vitrectomy.

Polymerase chain reaction

DNA was extracted from samples by use of a DNA Mini Kit (Qiagen, Valencia, CA, USA) installed on a robotic workstation for automated purification of nucleic acids (BioRobot E21, Qiagen). For the DNA extraction, approximately 0.1 ml aqueous humor and 0.2 ml vitreous fluid were used. DNA was eluted with 60 μl elution buffer, the amount of DNA used for PCR was 5 μl.

For the PCR assay, we used standard toxoplasma DNA strains for the *T. gondii* RH strains. To detect the toxoplasma genome (*T. gondii* B1 gene), we used two PCR assays, the qualitative multiplex PCR and the quantitative real-time PCR. Multiplex PCR was designed to qualitatively detect genomic DNA of human herpes viruses, i.e., herpes simplex virus type 1 (HSV-1) and type 2 (HSV-2), varicella zoster virus (VZV), Epstein–Barr virus (EBV), cytomegalovirus (CMV), and human herpes virus type 6 (HHV6), type 7 (HHV7), and type 8 (HHV8). PCR was performed using a LightCycler (Roche, Basel, Switzerland). Primers and probes of HHV1-8 and the PCR conditions have been described elsewhere [17, 18]. In addition to the herpes virus PCR, we calibrated the primers and the probe for detecting toxoplasma DNA (*T. gondii* B1 gene) as shown in Table 2. Specific primers for the virus were used with AccuPrime Taq (Invitrogen, Carlsbad, CA, USA). Products were subjected to 40 cycles of PCR amplification. Hybridization probes were then mixed with the PCR products. Real-time PCR was only performed for *T. gondii* when the genomic DNA of *T. gondii* was detected by multiplex screening PCR.

The real-time PCR was performed using AmpliTaq Gold and the Real-Time PCR 7300 system (Applied Biosystems, Foster City, CA, USA). The PCR conditions used for the *T. gondii* B1 gene were: 95°C for 0 s and 60°C for 20 s for 50 cycles. The PCR conditions used for the human herpes viruses have been described elsewhere [17, 18]. When more than 10 copies/mL were detected, the sample copy number was regarded as significant.

Results

Figure 1 shows representative PCR data (Case 1, Table 3). The multiplex PCR performed in order to screen all 8

Table 1 Clinical findings at initial presentation for patients with ocular toxoplasmosis

Case	Age	Sex	Eye	Initial findings and inflammation of AC					Duration of the symptoms	Vitreitis	Retinal vasculitis	Retinal exudates	
				VA	IOP (mmHg)	Granulomatous KPs	AC: cell	AC: flare				Old	Fresh
1	58	M	L	0.1	19	+	3+	131	2 months	+	+	+	+
2	70	F	L	0.3	21	+	2+	76	3 weeks	+	−	+	+
3	68	F	R	0.8	14	−	2+	34	2 months	+	+	−	+
4	44	M	R	1.0	12	+	1+	17	1.5 months	+	−	+	+
5	56	M	L	0.7	22	+	2+	43	3 weeks	+	+	+	+
6	65	F	L	1.0	15	+	1+	26	2 weeks	+	−	−	+
7	48	M	R	0.4	14	+	3+	124	3 weeks	+	+	+	+
8	35	M	L	0.6	18	−	1+	14	1 month	+	+	+	+
9	49	M	L	0.9	18	+	2+	29	1 month	+	+	+	+
10	59	F	R	0.5	20	−	1+	23	1.5 months	+	−	+	+
11	47	M	R	1.2	17	−	−	8	None	−	−	+	−
12	53	F	L	1.2	13	−	−	12	None	−	−	+	−
13	71	M	R	0.9	16	−	−	11	None	−	−	+	−

All patients were immunocompetent. "Old retinal exudates" indicates inactive ocular toxoplasmosis lesions in the form of old pigmented retinal scars

VA visual acuity, *IOP* intraocular pressure, *KPs* keratic precipitates, *AC* anterior chamber

Table 2 Design of primers and probe for detecting toxoplasma DNA (*T. gondii* B1 gene)

For multiplex PCR (qualitative PCR)
Primer F—TCCCCTCTGCTGGCGAAAAGT
Primer R—AGCGTTCGTGGTCAACTATCGATTG
LCRed640—GGTGTATTCGCAGATTGGTCGCCTG-P
Probe—CGAAAAGTGAAATTCATGAGTATCTGTG CAACT-6FAM
For Real-time PCR (quantitative PCR)
Primer F—TCCCCTCTGCTGGCGAAAAGT
Primer R—AGCGTTCGTGGTCAACTATCGATTG
Probe—6FAM-TCTGTGCAACTTTGGTGTATTCGCAG-iowaBK

We designed the primers and probes for the multiplex PCR and real-time PCR. The design of the primers is the same for the two PCR methods, although the relative positions of the TaqMan probe in the B1 gene were changed

human herpes virus DNAs and the *T. gondii* DNAs were positive for the *T. gondii* DNA (Fig. 1a). However, this sample was negative for all human herpes virus DNA tests. In addition, quantitative real-time PCR revealed that there were 1.1×10^6 copies/mL of *T. gondii* DNA in this specimen (Fig. 1b). Figure 2 shows the ocular findings for the patient. At the initial presentation, we made a clinical diagnosis of ocular toxoplasmosis based on both the clinical features and the serological tests (serum anti-Toxo IgG: ×640). Based on these findings, we treated the patient with systemic acetylspiramycin and prednisolone for 3 months. The treatment was effective and the active ocular lesions in the left eye completely disappeared. Two months after the treatment, a subsequent PCR indicated that the *T. gondii* DNA in the aqueous humor sample was now undetectable.

Table 3 summarizes the PCR results. Qualitative multiplex PCR for the *T. gondii* B1 gene was positive for 11 out of 13 patients with clinically suspected ocular toxoplasmosis (Table 3). Real-time PCR detected the B1 gene but not the human herpes virus DNA in the 10 patients who were clinically suspected of having ocular toxoplasmosis (10/13, 77%). In addition, high copy numbers of *T. gondii* DNA were detected (5.1×10^2–2.1×10^6 copies/mL) in all of these 10 patients, with active ocular inflammatory lesions that were compatible with ocular toxoplasmosis, i.e., focal retinal necrosis, vitreous opacity, anterior chamber cells, and choroidal edema with possible old scars. The only factors in the three PCR-negative patients that were compatible with an ocular toxoplasmosis diagnosis were the inactive scar lesions, i.e., old pigmented retinal scars. Of note is the finding that in one of these three patients *T. gondii* DNA was detected by the multiplex qualitative PCR in the aqueous humor sample (Case 12 in Table 3), even though the real-time PCR showed negative results (<10 copies/mL). A fundus photograph of a patient with inactive ocular toxoplasmosis is seen in Fig. 3. For this particular patient (Case 11 in Table 3), the PCR results

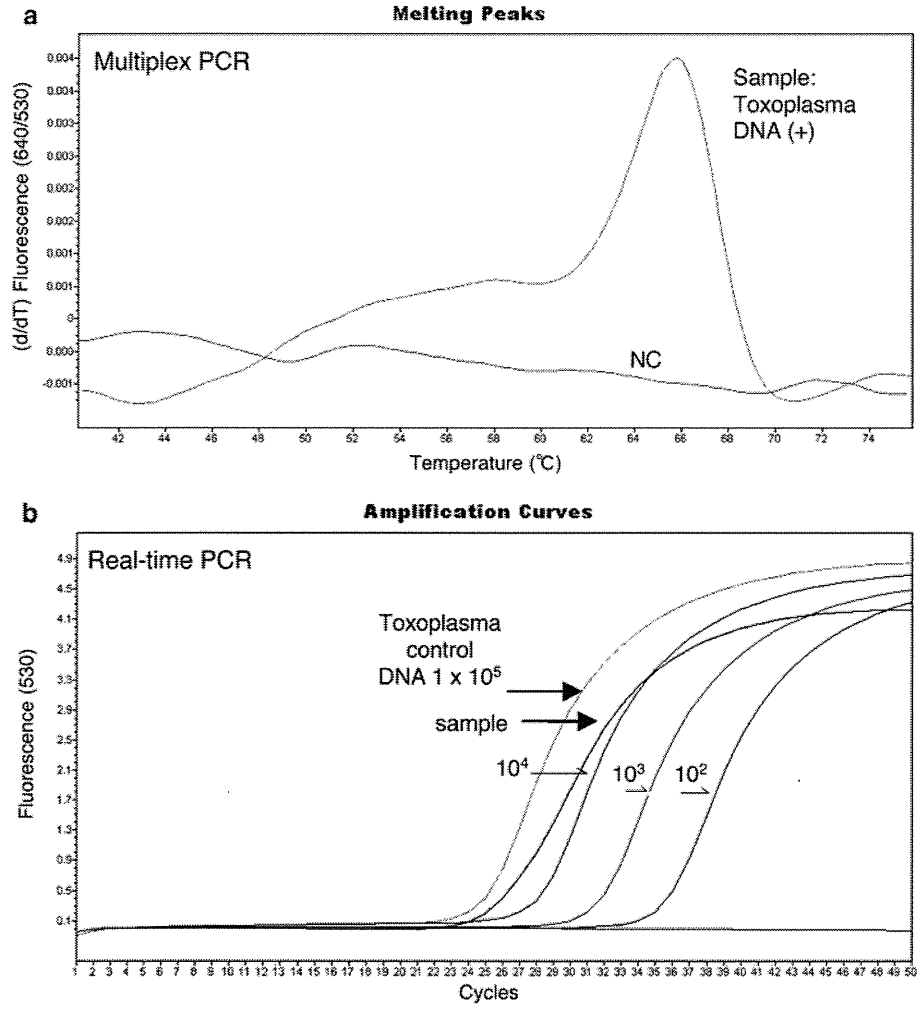

Fig. 1 PCR results for a patient with ocular toxoplasmosis (Case 1 in Table 3). **a** After DNA extraction from the sample, multiplex PCR was performed to screen for *T. gondii*, and for HHV1 to HHV8 using LightCycler capillaries. At 66°C, a significant positive curve was detected, indicating the detection of *T. gondii* genomic DNA in the aqueous humor. Using other LightCycler capillaries, human herpes viruses HSV1, HSV2, VZV, EBV, CMV, HHV6, HHV7, and HHV8 were negative for this sample. The flat line indicates the negative control. **b** Quantitative real-time PCR of the same sample shown in **a**. We calculated the copy number of the *T. gondii* genomic DNA in the sample. We measured both the tested ocular sample and control DNA (10^5, 10^4, 10^3, and 10^2 copies/mL) by real-time PCR, and then established the standard curve using the results of the control DNA. The standard curve was used to calculate the DNA concentration for the cycle threshold (*Ct*) value of the sample. The final copy number of genomic DNA in the sample (copies/mL) was calculated on the basis of the obtained sample volume and final dilution volume. Values were regarded as significant when more than 10 copies/mL were observed. The real-time PCR revealed there were 1.1×10^6 copies/mL of *T. gondii* DNA in this analyzed sample

were negative. In the serum of all of the ocular toxoplasmosis patients, the anti-toxoplasma IgG was positive (Table 3).

Negative PCR results were obtained for all the control uveitis patient samples (Cases 14–23 in Table 3) and for the control non-uveitis patients (data not shown).

Discussion

Using intraocular fluids for PCR gene amplification is helpful in diagnosing various ocular diseases, because it is possible to detect an exceedingly small amount of nucleic acid in a small ocular sample volume with high sensitivity. We report here a new PCR assay system that uses two separate steps, multiplex screening PCR and quantitative real-time PCR. With this new system, it becomes possible to detect *T. gondii* and rule out human herpes virus-related necrotizing retinitis. For these two PCR analyses in this study, oligonucleotide primers and a TaqMan probe were designed to amplify the *T. gondii* B1 gene. Our results clearly demonstrate that the PCR assay system succeeded in detecting the *T. gondii* DNA in the ocular fluid samples of the 10 patients with active ocular toxoplasmosis lesions,

Table 3 Detection of *T. gondii* DNA by qualitative multiplex PCR and quantitative real-time PCR in ocular samples from clinically suspected ocular toxoplasmosis

Case	Disease	Sample	Multiplex PCR	Real-time PCR (copies/mL)	Serum anti-Toxo IgG	Treatment
1	Toxoplasmosis (active)	AH	*T. gondii* DNA+	*T. gondii* DNA: 1.1×10^6	640	ASPM, PSL
2	Toxoplasmosis (active)	AH	*T. gondii* DNA+	*T. gondii* DNA: 1.6×10^3	320	ASPM
3	Toxoplasmosis (active)	AH	*T. gondii* DNA+	*T. gondii* DNA: 5.1×10^2	640	ASPM, PSL
4	Toxoplasmosis (active)	AH	*T. gondii* DNA+	*T. gondii* DNA: 3.0×10^4	2560	ASPM, PSL
5	Toxoplasmosis (active)	AH	*T. gondii* DNA+	*T. gondii* DNA: 9.4×10^4	5120	ASPM, PSL
6	Toxoplasmosis (active)	AH	*T. gondii* DNA+	*T. gondii* DNA: 5.5×10^4	2560	ASPM, PSL
7	Toxoplasmosis (active)	AH	*T. gondii* DNA+	*T. gondii* DNA: 9.9×10^2	640	CLDM
8	Toxoplasmosis (active)	VF	*T. gondii* DNA+	*T. gondii* DNA: 1.1×10^4	640	ASPM, PSL, PPV
9	Toxoplasmosis (active)	AH	*T. gondii* DNA+	*T. gondii* DNA: 4.2×10^3	2560	ASPM, PSL
10	Toxoplasmosis (active)	VF	*T. gondii* DNA+	*T. gondii* DNA: 2.1×10^6	1280	ASPM, PSL, PPV
11	Toxoplasmosis (old)	AH	–	<10	2560	None
12	Toxoplasmosis (old)	AH	*T. gondii* DNA+	<10	320	CLDM
13	Toxoplasmosis (old)	AH	–	<10	640	None
14	Idiopathic uveitis	AH	–	<10	320	None
15	Acute retinal necrosis	VF	VZV DNA+	VZV DNA: 8.3×10^6	<160	Valaciclovir, PPV, PSL
16	CMV retinitis	AH	CMV DNA+	CMV DNA: 9.0×10^5	<160	Ganciclovir
17	Idiopathic uveitis	AH	–	<10	<160	None
18	Idiopathic uveitis	VF	–	<10	<160	PSL, PPV
19	Idiopathic uveitis	AH	–	<10	<160	None
20	Acute retinal necrosis	AH	VZV DNA+	VZV DNA: 9.9×10^5	<160	Valaciclovir, PSL
21	Idiopathic uveitis	AH	–	<10	<160	PSL
22	Idiopathic uveitis	AH	–	<10	1280	PSL
23	Idiopathic uveitis	AH	–	<10	<160	None

We performed two PCR examinations using qualitative multiplex PCR and quantitative real-time PCR. Qualitative multiplex PCR was performed to screen for detection of the DNA of human herpes virus (HHV1-HHV8) and *T. gondii*. All samples from ocular toxoplasmosis (Cases 1–13) were negative for HHV-DNA. Anti-toxoplasma IgG was positive in the serum of all ocular toxoplasmosis patients. We collected a second ocular sample from cases 1, 2, 6, 7, 8, and 10, and performed PCR examinations. The results were all negative for DNA of human herpes virus and *T. gondii*

AH aqueous humor, *ASPM* acetylspiramycin, *CLDM* clindamycin, *PPV* pars plana vitrectomy, *PSL* prednisolone, *VF* vitreous fluids

but not in the three samples with inactive lesions. In addition, PCR did not detect any of the human herpes virus DNAs in any of the samples, nor did these PCR methods detect *T. gondii* DNA in any of the control patients. These results therefore suggest that when intraocular fluid samples are examined by a sequence of multiplex PCR and real-time PCR, the results can be used to diagnose ocular toxoplasmosis.

In this study, there was one case (Case 12 in Table 3) for which the results were positive when using qualitative multiplex PCR and negative when using quantitative real-time PCR. The qualitative PCR examination is extremely sensitive and, as such, is able to detect DNA released from inactive parasites. This may be the reason for the discrepancy seen between the qualitative and quantitative assays. However, because the amounts of intraocular DNA are so low in such patients, these situations can be regarded as innocuous. Thus, when attempting to diagnose patients, both qualitative PCR and quantitative real-time PCR should be performed to ensure that any positive results are a result of active disease and not related to older non-active lesions. When using real-time PCR, we found there was a correlation between the high DNA loads in the ocular fluids, which translates as a high copy number of *T. gondii* DNA, and the intraocular inflammation in the uveitis patients with ocular toxoplasmosis. In fact, the case that was positive when using qualitative PCR and negative when using real-time PCR (Case 12) turned out to be a patient with inactive uveitis (old pigmented retinal exudates without inflammatory signs). In this particular case, before determining the actual reason for the positivity, we did administer clindamycin to the patient in order to prevent any possible recurrence.

Although both the Goldmann–Witmer coefficient (GWC) and PCR are useful for clinical specimen analyses [1–16] and can achieve similar levels of assay sensitivity,

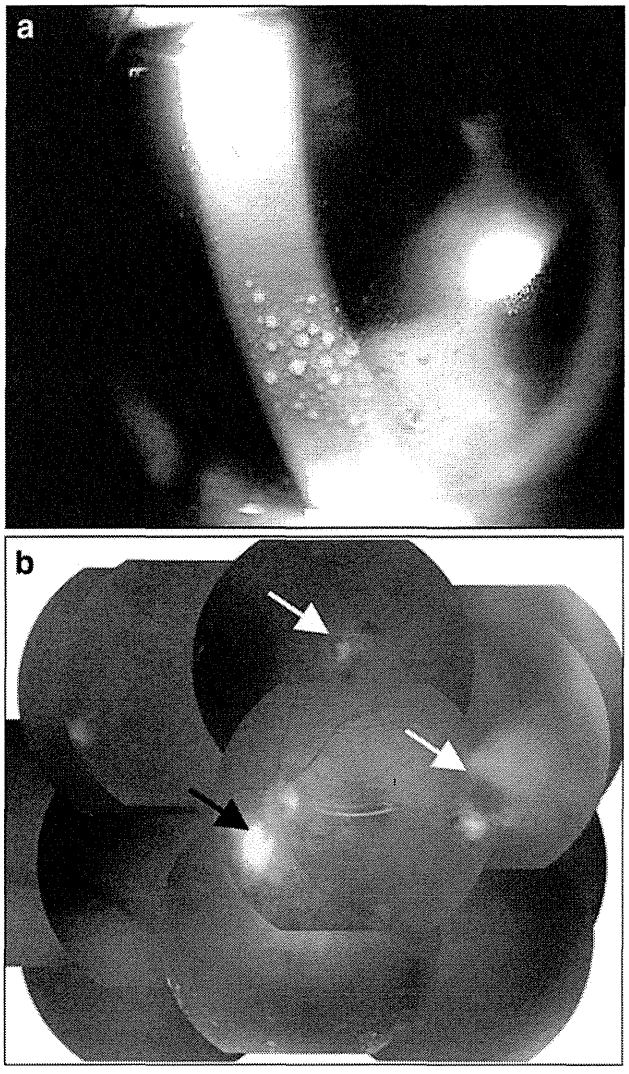

Fig. 2 Fundus and slit photograph of a patient with ocular toxoplasmosis (Case 1 in Table 3). **a** Slit and fundus photograph. **b** OS of a patient with an active toxoplasmosis infection. Diffuse keratic precipitates and anterior chamber cells (*upper panel*), and retinal yellowish white mass lesions (Edmund–Jensen type: *black arrow*) and retinal-pigmented exudates (*white arrows*) together with vitreous opacities are seen (*lower panel*)

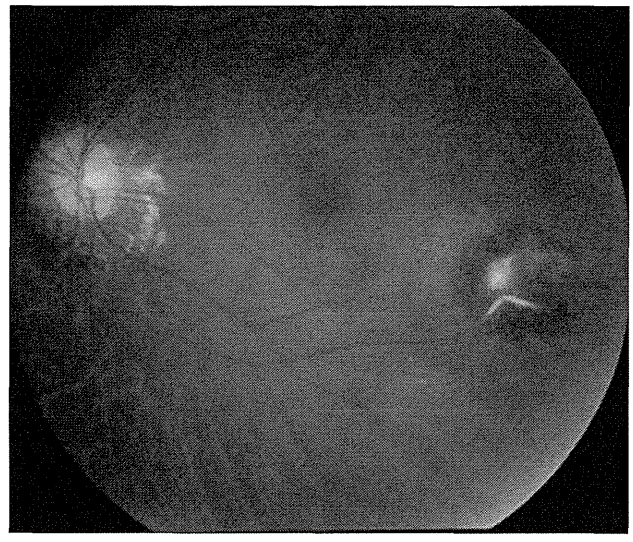

Fig. 3 A fundus photograph OS from an inactive ocular toxoplasmosis patient (Case 11 in Table 3). Old pigmented retinal exudates without inflammatory signs (vitreous cells, vitreous opacity, or retinal vasculitis) can be seen. PCR assay results were negative for genomic DNA of *T. gondii*

the proposed PCR system may be more advantageous since it has the ability to quantify the infection load of a clinical specimen. In addition, PCR examinations can exclude other major ocular infections that are caused by the human herpes virus. Westeneng et al. [7] reported 10 cases of ocular toxoplasmosis in immunocompromised patients. The PCR results were initially negative in 6 of these patients, with diagnosis only confirmed after use of the GWC. On the other hand, de Boer et al. report the use of PCR analysis was preferred for immunocompromised patients, because production of the local specific antibodies can be unpredictable in such patients [10]. Although the use of either PCR or GWC to diagnose ocular toxoplasmosis remains controversial, we were able to use PCR to detect the genomic DNA of toxoplasmosis in our immunocompetent patients even when they only had an active ocular inflammation. Therefore, this PCR methodology may be useful for *T. gondii* infection screening when used in conjunction with other diagnostic techniques, for example routine serological tests. In this study, we found increased anti-toxoplasma IgG in the serum of all of the ocular toxoplasmosis patients. However, we also found increased anti-toxoplasma IgG in the serum of two of our uveitis patients without ocular toxoplasmosis (Cases 14 and 22 in Table 3). We therefore recommend that PCR also be used to measure the toxoplasma DNA in ocular samples.

The protozoan parasite *T. gondii* has emerged as an important opportunistic infectious pathogen. In the eye, *T. gondii* infections can cause granulomatous pan-uveitis and necrotic retinitis, with typical ocular inflammation indicative of focal retinal necrosis, vitreous opacity, anterior chamber cells, and choroidal edema. Fundus lesions seen in ocular toxoplasmosis can be atypical in many patients, resembling necrotizing retinitis caused by human herpes viruses. The new PCR method is particularly useful when screening those uveitis patients who usually fail to generate specific IgM or increased IgG titers for *T. gondii* or who have had focal retinal necrosis. Thus, these results can be used to distinguish the findings from other retinal necrotic disorders, for example acute retinal necrosis and cytomegalovirus retinitis. By using several different primer pairs in LightCycler capillaries, these methods proved capable of rapidly screening for detection of the genome of

all eight types of human herpes virus and *T. gondii*. Development of this multiplex and real-time PCR assay seems to be quite advantageous, because this methodology makes it possible to exclude non-toxoplasma uveitis patients.

In conclusion, we have established a rapid, sensitive, comprehensive, two-step PCR system that can be used to detect *T. gondii*. New studies that examine larger numbers of samples from suspected ocular toxoplasmosis patients will need to be undertaken in the future in order to definitively establish the clinical value of this new diagnostic technique.

Acknowledgments Drs Kazuichi Maruyama and Kenji Nagata of the Department of Ophthalmology, Kyoto Prefectural University of Medicine, collected and sent the samples used in this study. We are grateful for the expert technical assistance of Mr Ken Watanabe. This work was supported by Comprehensive Research on Disability, Health and Welfare, Health and Labour Sciences Research Grants, Ministry Health, Labour and Welfare, Japan.

References

1. Aouizerate F, Cazenave J, Poirier L, Verin P, Cheyrou A, Begueret J, et al. Detection of *Toxoplasma gondii* in aqueous humour by the polymerase chain reaction. Br J Ophthalmol. 1993;77:107–9.
2. Manners RM, O'Connell S, Guy EC, Joynson DH, Canning CR, Etchells DE. Use of the polymerase chain reaction in the diagnosis of acquired ocular toxoplasmosis in an immunocompetent adult. Br J Ophthalmol. 1994;78:583–4.
3. Robert-Gangneux F, Binisti P, Antonetti D, Brezin A, Yera H, Dupouy-Camet J. Usefulness of immunoblotting and Goldmann–Witmer coefficient for biological diagnosis of toxoplasmic retinochoroiditis. Eur J Clin Microbiol Infect Dis. 2004;23:34–8.
4. De Groot-Mijnes JD, Rothova A, Van Loon AM, Martinus RA, Völker R, ten Dam-van Loon NH, et al. Polymerase chain reaction and Goldmann–Witmer coefficient analysis are complimentary for the diagnosis of infectious uveitis. Am J Ophthalmol. 2006;141:313–8.
5. Kijlstra A, Luyendijk L, Baarsma GS, Rothova A, Schweitzer CM, Timmerman Z, et al. Aqueous humor analysis as a diagnostic tool in toxoplasma uveitis. Int Ophthalmol. 1989;13:383–6.
6. Witmer R. Clinical implications of aqueous humor studies in uveitis. Am J Ophthalmol. 1978;86:39–44.
7. Westeneng AC, Rothova A, de Boer JH, de Groot-Mijnes JD. Infectious uveitis in immunocompromised patients and the diagnostic value of polymerase chain reaction and Goldmann–Witmer coefficient in aqueous analysis. Am J Ophthalmol. 2007;144:781–5.
8. Matos K, Muccioli C, Belfort Junior R, Rizzo LV. Correlation between clinical diagnosis and PCR analysis of serum, aqueous, and vitreous samples in patients with inflammatory eye disease. Arq Bras Oftalmol. 2007;70:109–14.
9. Rothova A, de Boer JH, Ten Dam-van Loon NH, Postma G, de Visser L, Zuurveen SJ, et al. Usefulness of aqueous humor analysis for the diagnosis of posterior uveitis. Ophthalmology. 2008;115:306–11.
10. de Boer JH, Verhagen C, Bruinenberg M, Rothova A, de Jong PT, Baarsma GS, et al. Serologic and polymerase chain reaction analysis of intraocular fluids in the diagnosis of infectious uveitis. Am J Ophthalmol. 1996;121:650–8.
11. Figueroa MS, Bou G, Marti-Belda P, Lopez-Velez R, Guerrero A. Diagnostic value of polymerase chain reaction in blood and aqueous humor in immunocompetent patients with ocular toxoplasmosis. Retina. 2000;20:614–9.
12. Bottós J, Miller RH, Belfort RN, Macedo AC, UNIFESP Toxoplasmosis Group, Belfort R Jr, et al. Bilateral retinochoroiditis caused by an atypical strain of *Toxoplasma gondii*. Br J Ophthalmol. 2009;93:1546–50.
13. Lin MH, Chen TC, Kuo TT, Tseng CC, Tseng CP. Real-time PCR for quantitative detection of *Toxoplasma gondii*. J Clin Microbiol. 2000;38:4121–5.
14. Patrat-Delon S, Gangneux JP, Lavoué S, Lelong B, Guiguen C, le Tulzo Y, et al. Correlation of parasite load determined by quantitative PCR to clinical outcome in a heart transplant patient with disseminated toxoplasmosis. J Clin Microbiol. 2010;48:2541–5.
15. Fekkar A, Bodaghi B, Touafek F, Le Hoang P, Mazier D, Paris L. Comparison of immunoblotting, calculation of the Goldmann–Witmer coefficient, and real-time PCR using aqueous humor samples for diagnosis of ocular toxoplasmosis. J Clin Microbiol. 2008;46:1965–7.
16. Cassaing S, Bessières MH, Berry A, Berrebi A, Fabre R, Magnaval JF. Comparison between two amplification sets for molecular diagnosis of toxoplasmosis by real-time PCR. J Clin Microbiol. 2006;44:720–4.
17. Sugita S, Shimizu N, Watanabe K, Mizukami M, Morio T, Sugamoto Y, et al. Use of multiplex PCR and real-time PCR to detect human herpes virus genome in ocular fluids of patients with uveitis. Br J Ophthalmol. 2008;92:928–32.
18. Sugita S, Iwanaga Y, Kawaguchi T, Futagami Y, Horie S, Usui T, et al. Detection of herpesvirus genome by multiplex polymerase chain reaction (PCR) and real-time PCR in ocular fluids of patients with acute retinal necrosis. Nippon Ganka Gakkai Zasshi. 2008;112:30–8.
19. Sugita S, Shimizu N, Watanabe K, Katayama M, Horie S, Ogawa M, et al. Diagnosis of bacterial endophthalmitis by broad-range quantitative polymerase chain reaction. Br J Ophthalmol. 2011;95:345–9.

Graefes Arch Clin Exp Ophthalmol (2012) 250:391–398
DOI 10.1007/s00417-011-1819-1

INFLAMMATORY DISORDERS

Detection of *Candida* and *Aspergillus* species DNA using broad-range real-time PCR for fungal endophthalmitis

Sunao Sugita · Koju Kamoi · Manabu Ogawa · Ken Watanabe · Norio Shimizu · Manabu Mochizuki

Received: 24 June 2011 / Revised: 29 August 2011 / Accepted: 2 September 2011 / Published online: 27 September 2011

Abstract
Background The goal of this work is to establish a broad-range real-time polymerase chain reaction (PCR) diagnostic system for ocular fungal infection and to measure *Candida* and *Aspergillus* DNA in the ocular fluids obtained from unknown uveitis/endophthalmitis patients.
Methods After obtaining informed consent, intraocular fluids (aqueous humor and vitreous fluid samples) were collected from 54 patients with idiopathic uveitis or endophthalmitis. Samples were assayed for *Candida* or *Aspergillus* DNA using broad-range (18S rRNA sequences) quantitative real-time PCR.
Results *Candida* or *Aspergillus* DNA was detected in seven out of 54 patient ocular samples (13%). These PCR-positive samples showed significantly high copy numbers of *Candida* or *Aspergillus* DNA. On the other hand, fungal DNA was not detected in any of the other 46 samples collected from these idiopathic uveitis or endophthalmitis patients. In the one PCR-negative case, PCR did not detect any fungal genome in the sample, even though this patient was clinically suspected of having *Candida* endophthalmitis. Real-time PCR results were negative for fungal DNA in the bacterial endophthalmitis patients and in various uveitis patients. In addition, fungal DNA was also not detected in patients without ocular inflammation (controls).
Conclusions Analysis of ocular samples by this broad-range real-time PCR method can be utilized for rapid diagnosis of patients suffering from unknown intraocular disorders such as idiopathic uveitis/endophthalmitis.

Keywords Endophthalmitis · Fungal infection · Polymerase chain reaction

S. Sugita (✉) · K. Kamoi · M. Ogawa · M. Mochizuki
Department of Ophthalmology & Visual Science,
Tokyo Medical and Dental University,
Graduate School of Medical and Dental Sciences,
1-5-45 Yushima,
Bunkyo-ku, Tokyo 113-8519, Japan
e-mail: sunaoph@tmd.ac.jp

K. Watanabe · N. Shimizu
Department of Virology, Division of Medical Science,
Tokyo Medical and Dental University,
Graduate School of Medical and Dental Sciences,
Tokyo, Japan

Introduction

Fungal endophthalmitis is a sight-threatening disease caused by human pathogenic fungi. Fungal infections are known to cause ocular inflammations such as endophthalmitis, uveitis, and keratitis. However, with the exception of for the *Candida*-associated ocular infection, the association between the fungus and the observed clinical features has yet to be elucidated. The well-known clinical features for *Candida* endophthalmitis include a fungal ball in the retina and vitreous opacity [1]. Fungal endophthalmitis can result from hematogenous dissemination or from a direct inoculation following trauma or surgery to the eye. Risk factors for fungal endophthalmitis include intravascular catheters, diabetes, malignancy, chemotherapeutic agents, and steroids. However, the clinical findings can be very diverse in some cases of ocular inflammatory disorders caused by fungal species. Moreover, fungal infections have been widely associated with keratitis, retinitis, uveitis, retinal/choroidal vasculitis, invasive orbital infection, and endophthalmitis. Because of this diversity, infection diagnosis is both difficult and time-consuming [1–4]. In order to be able to perform adequate treatments that can prevent these infectious agents from causing irreversible ocular damage,

early examinations that correctly identify the etiology of the infection are necessary.

Conventional methods of diagnosis of fungal endophthalmitis include detection and isolation of the fungi from the intraocular fluids (aqueous humor or vitreous). However, since the sensitivity of conventional fungal cultures is not high, and the culture growth rates are slow, longer times are required before final results can be obtained [5, 6]. Thus, an early diagnosis can be important in ensuring there is prompt management of the endophthalmitis. Previous studies have shown that polymerase chain reaction (PCR) can be successfully and reliably used to make a diagnosis of fungal endophthalmitis [7–10]. However, even conventional PCR has yet to be able to determine quantitative information for the fungal genome in ocular samples.

In this study, we used real-time quantitative PCR for detection of *Candida* and *Aspergillus* DNA. We developed a protocol for the rapid detection of fungal DNA in ocular samples that was based on two major species (*Candida* and *Aspergillus*) that commonly cause eye disorders. We designed novel panfungal primers and probes that were complementary to the 18S rRNA sequences present in these species. Our broad-range real-time PCR proved to be an accurate method for quantitating fungal copies of both *Candida* and *Aspergillus* DNA.

Methods

Sample preparation

From 2006 to 2010, we consecutively enrolled endophthalmitis and uveitis patients in a prospective study that was conducted at our hospital (Table 1). After informed consent was obtained in all patients, we collected aqueous humor and vitreous fluid samples. A 0.1–0.2 ml aliquot of aqueous humor (asepsis) was collected in a syringe with a 30-G needle. We also collected non-diluted vitreous fluid samples (0.5–1.0 ml) during diagnostic pars plana vitrectomy (PPV) procedures that were conducted in patients with clinically suspected fungal endophthalmitis/uveitis. All of the patients displayed active intraocular inflammation at the time of sampling. The samples were transferred into a pre-sterilized microfuge tube and used for PCR. To ensure that no contamination of the PCR preparation occurred, the DNA amplification and the analysis of the amplified products were done in separate laboratories, as per a method reported for one of our previous studies [11].

For cultures of fungi, the Bacteria Work Station of the Tokyo Medical and Dental University Hospital processed all specimens (aqueous humor and vitreous fluids) within 1 h after the sample collection, with standard methods followed for the isolation and identification of fungal cultures [11].

In addition to the patient groups, we also analyzed samples from a control group. A total of 40 samples (20 aqueous humor and 20 vitreous fluids) were collected from patients who did not have any type of ocular inflammation (age-related cataract, macular edema, retinal detachment, idiopathic macular hole, or idiopathic epiretinal membrane).

The research followed the tenets of the Declaration of Helsinki and all study protocols were approved by the Institutional Ethics Committee of Tokyo Medical and Dental University. This clinical trial was registered, with registration information available at www.umin.ac.jp/ctr/index/htm. The study number attached to this registration is R000002708. The study was begun in April of 2006 and ended in April of 2010.

Polymerase chain reaction

To detect the *Candida* and *Aspergillus* DNA, we designed primers and probes for the broad-range PCR of the 18S rRNA sequences, which we have described in a previous report [10]. Kami et al. [12] developed primers and a probe for real-time PCR and demonstrated that the procedure was highly specific for the *Aspergillus* infection. In this study, we also designed a probe for use in the *Candida* species DNA amplifications (Fig. 1).

DNA was extracted from the samples using a DNA Mini Kit (Qiagen, Valencia, CA) installed on a robotic workstation that was set for automated purification of nucleic acids (BioRobot E21, Qiagen). The real-time PCR was performed using the Amplitaq Gold and the Real-Time PCR 7300 system (Applied Biosystems, Foster City, CA) or Light Cycler 480 II (Roche, Switzerland). The paired primers and TaqMan probes used for *Candida* and *Aspergillus* are shown in Fig. 1. Products were subjected to 50 cycles of PCR amplification, with cycling conditions set at 95°C for 10 min, followed by 50 cycles at 95°C for 15 s and 60°C for 1 min. For PCR assay sensitivity, PCR fragments were amplified from the DNA of *C. albicans* (Strain: ATCC 60193). Amplification of the human β-globulin gene served as an internal positive extraction and amplification control. Copy number values of more than ten copies/ml in the sample were considered to be significant.

Results

Specificity of *Candida* and *Aspergillus* species in broad-range real-time PCR

To evaluate the specificity of the *Candida* and *Aspergillus* species using broad-range real-time PCR of the 18S rRNA sequences, total nucleic acids of six *Candida* species and five *Aspergillus* species were extracted and assayed for 18S

Table 1 Detection of *Candida* and *Aspergillus* 18S rRNA gene by broad-range real-time PCR in unknown uveitis or endophthalmitis patients and control uveitis patients

Initial diagnosis	No. of patients	Sample	Results for real-time PCR	Final diagnosis	Remarks
Idiopathic uveitis/ endophthalmitis	n=46	Aqh, VF	<10 copies	Idiopathic uveitis/ endophthalmitis	
	n=1 (65, male)	VF	*Candida* 9.2×10^5 copies/ml	*Candida* endophthalmitis	Case 1; Endogenous endophthalmitis
	n=1 (71, female)	VF	*Aspergillus* 4.5×10^2 copies/ml	*Aspergillus* endophthalmitis	Case 2; Endogenous endophthalmitis
	n=1 (73, male)	VF	*Aspergillus* 1.8×10^3 copies/ml	*Aspergillus* endophthalmitis	Case 3; Late postoperative endophthalmitis
	n=1 (80, male)	Aqh	*Candida* 3.4×10^2 copies/ml	*Candida* endophthalmitis	Case 4; Post-traumatic corneal ulceration
	n=1 (66, female)	VF	*Candida* 6.5×10^5 copies/ml	*Candida* endophthalmitis	Case 5; Endogenous endophthalmitis (IFN treatment)
	n=1 (74, male)	VF	*Candida* 6.2×10^4 copies/ml	*Candida* endophthalmitis	Case 6; Endogenous endophthalmitis (diabetes)
	n=1 (0, female)	VF	*Candida* 9.4×10^4 copies/ml	*Candida* endophthalmitis	Case 7; Endogenous endophthalmitis (normal infant)
	n=1 (60, male)	Aqh	<10 copies	*Candida* endophthalmitis	Case 8; Endogenous endophthalmitis (IVH use)
Bacterial endophthalmitis	n=7	Aqh, VF	<10 copies	/	
Sarcoidosis	n=4	Aqh, VF	<10 copies	/	
Vogt-Koyanagi-Harada disease	n=1	Aqh	<10 copies	/	
Toxocariasis	n=1	Aqh	<10 copies	/	
Toxoplasmosis	n=3	Aqh, VF	<10 copies	/	
Acute retinal necrosis	n=7	Aqh, VF	<10 copies	/	
Cytomegalovirus retinitis	n=4	Aqh, VF	<10 copies	/	
Herpetic anterior iridocyclitis	n=4	Aqh	<10 copies	/	
Non-inflammatory ocular diseases*	n=40	Aqh, VF	<10 copies	/	Controls for PCR

*Non-inflammatory ocular diseases: age-related cataract, macular edema, retinal detachment, idiopathic macular hole or idiopathic epiretinal membrane

Aqh aqueous humor, *IFN* interferon, *IVH* Intravenous hyperalimentation, *VF* vitreous fluids

rDNA. As seen in Fig. 1, the broad-range real-time PCR detected six *Candida* species, i.e., *C. albicans, C. parapsilosis, C. tropicalis, C. guilliermondii, C. glabrata,* and *C. krusei*, along with five *Aspergillus* species, i.e., *A. fumigatus, A. flavus, A. nidulans, A. niger,* and *A. terreus*. By using several different primers and probes, we were able to separately detect each of these fungal species (Fig. 1).

Sensitivity of the real-time PCR assay

To confirm the broad-range real-time PCR assay sensitivity, PCR fragments were amplified from the DNA of *C. albicans*. The detection limit and standard range of the TaqMan real-time PCR were determined by using serial tenfold dilutions of linearized plasmid. The PCR results for the prepared samples showed that the best sensitivity for detecting *C. albicans* DNA was at a concentration of 10^1 per PCR (Fig. 2). There was no detection of the DNA in the negative control (nuclease-free water).

Detection of *Candida* and *Aspergillus* 18S rRNA gene in unknown uveitis/endophthalmitis patients

PCR results indicated a total of seven ocular fluid samples from the idiopathic uveitis or endophthalmitis patients (7/54, 13% positive, Table 1) were positive for *Candida* or *Aspergillus* DNA. These positive patients had high copy numbers of either *Candida* or *Aspergillus* DNA, with values ranging from 3.4×10^2 to 9.2×10^5 copies/ml. These results indicate the presence of a fungal infection. A representative PCR result is shown in Fig. 3. Conversely, conventional fungal cultures only found two out of the seven PCR-positive samples (both *C. albicans*) to be positive, while the other five samples were negative.

On the other hand, fungal DNA was not detected in any of the other 46 samples collected from these idiopathic uveitis or endophthalmitis patients. In the one PCR-negative case, PCR did not detect any fungal genome in the aqueous humor (<10 copies, case 8 in Table 1), even

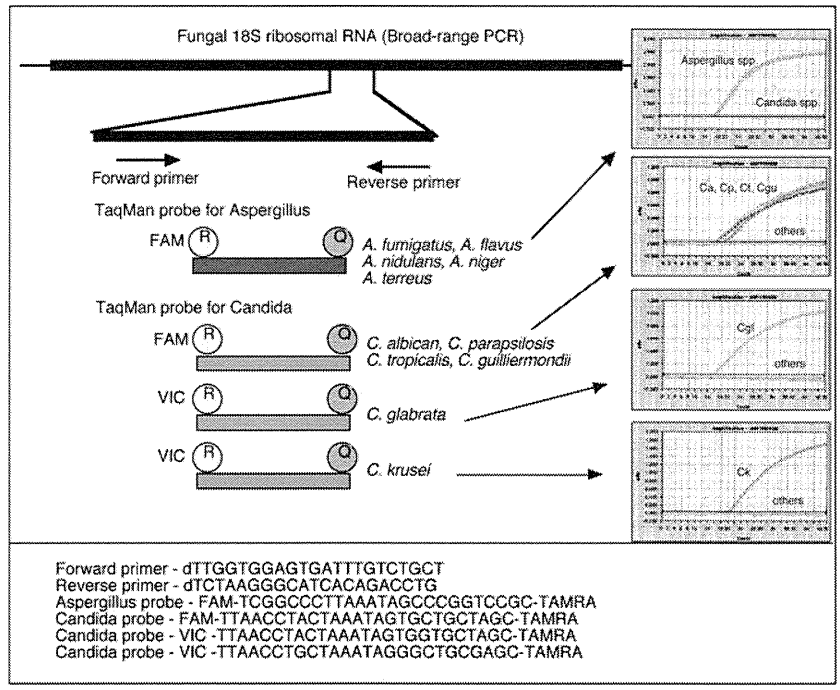

Fig. 1 Specific primers and probes for broad-range real-time PCR of the fungal 18S rRNA sequence were designed in order to detect DNA for *Candida* and *Aspergillus* species

though this patient was clinically suspected of having *Candida* endophthalmitis. Real-time PCR results were negative for the *Candida* and *Aspergillus* DNA in the bacterial endophthalmitis patients (n=7) and in the various uveitis patients (n=24) who had been diagnosed with sarcoidosis, Vogt-Koyanagi-Harada disease, toxocariasis, toxoplasmosis, acute retinal necrosis, cytomegalovirus retinitis, or herpetic anterior iridocyclitis. In addition, fungal DNA was not detected in any of the 40 control samples that were collected from the patients without ocular inflammation.

Of the seven patients who were PCR positive, further examinations led to fungal endophthalmitis diagnoses as follows: five patients had endogenous endophthalmitis (four *Candida* and one *Aspergillus*), one had late postoperative endophthalmitis (*Aspergillus*, case 3), and one had post-traumatic keratitis-associated endophthalmitis (*Candida*, case 4) (Table 1).

Case reports

Case 1

A 65-year-old man with type II diabetes mellitus was treated for unknown uveitis over a period of a few weeks during 2009. He complained of blurred vision, decreased visual acuity, and pain in his right eye (RE). Ophthalmologic examination demonstrated the presence of characteristics of uveitis, bacterial endophthalmitis and fungal endophthalmitis. Vitreous opacity, including the presence of a fungal ball and yellowish retinal exudates, was seen in the fundus of his RE (Fig. 4a). After vitrectomy of his RE,

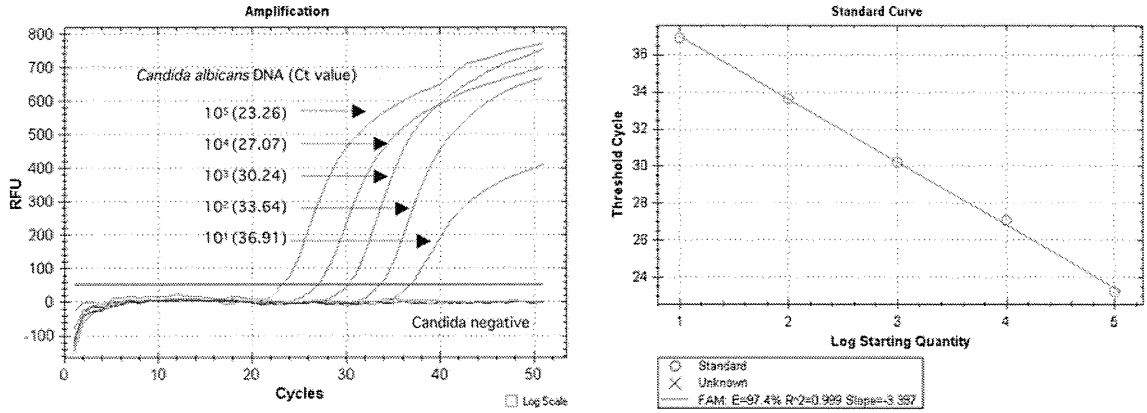

Fig. 2 In order to examine broad-range real-time PCR assay sensitivity for the fungal 18S PCR, the PCR fragments were amplified from the DNA of *C. albicans* (ATCC 60193). The *number in parenthesis* indicates the cycle threshold (Ct) value in quantitative PCR

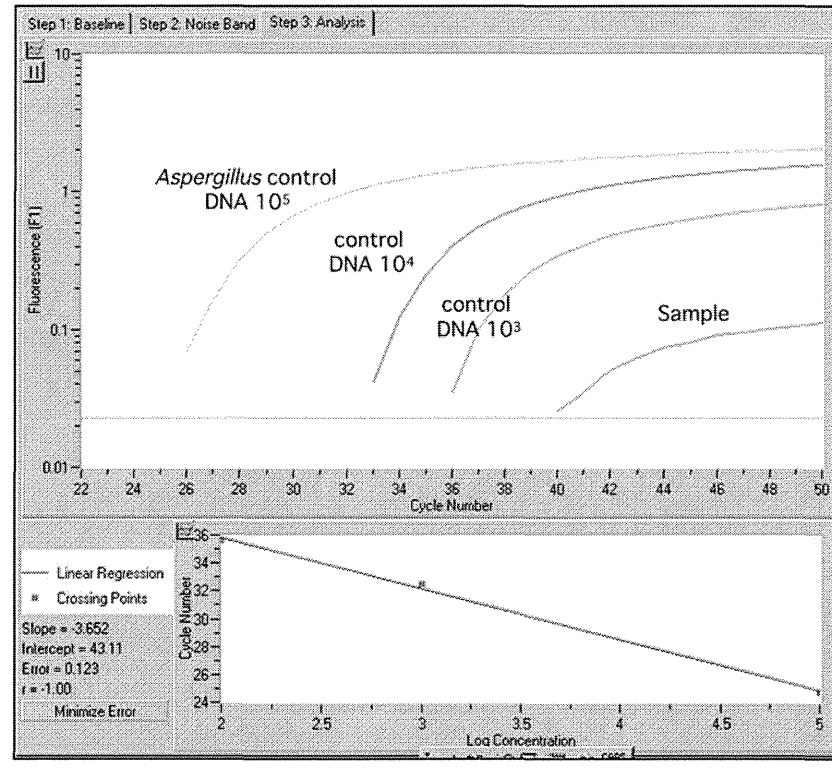

Fig. 3 Representative data for the broad-range real-time PCR. *Aspergillus* DNA (4.5×10^2 copies/ml) but not *Candida* DNA was detected in the vitreous sample of case 2

real-time PCR of the vitreous sample obtained during the procedure indicated there were high copy numbers of *Candida* DNA (9.2×10^5 copies/ml, Fig. 4b). Based on these results, the patient was given systemic fluconazole (Table 1). *Aspergillus* DNA was not detected in this sample. A few days later, fungal culture of his vitreous specimen

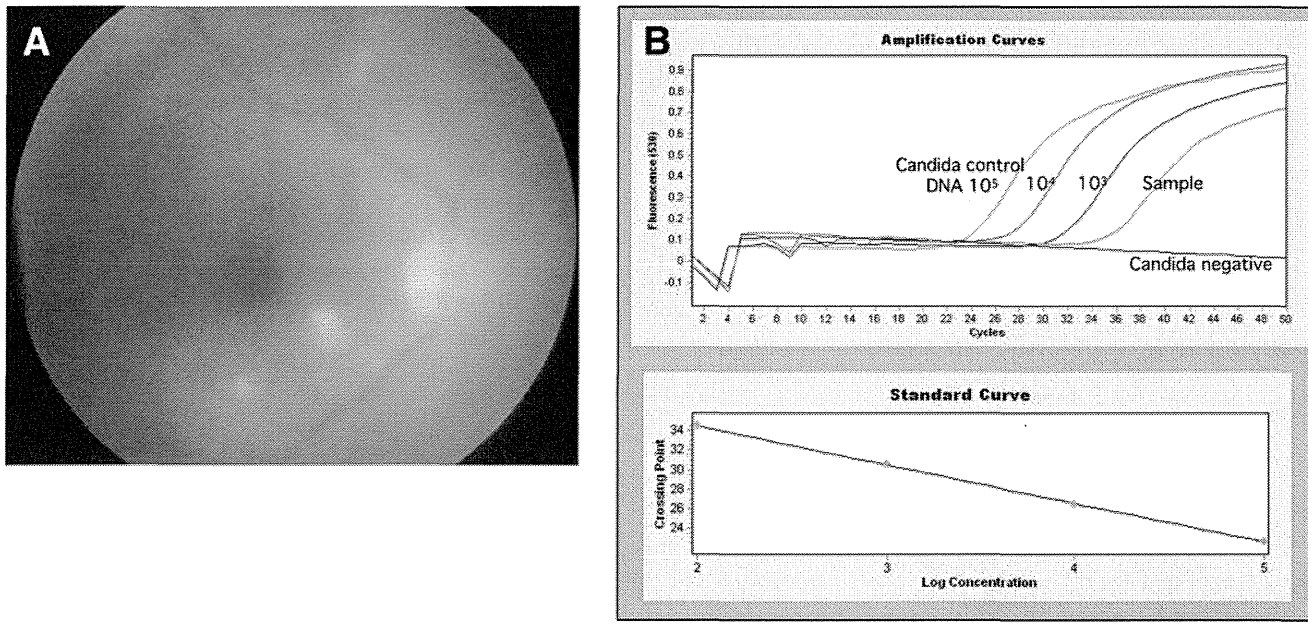

Fig. 4 PCR results for case 1. **a** Fundus photograph of the right eye with a *Candida* infection. Dense vitreous opacity and retinal exudates are seen. **b** This is a graph of the PCR results. We calculated the copy number of fungal genomic DNA in the sample. After we measured both the tested ocular sample and the control DNA (10^5, 10^4, and 10^3 copies/ml) using real-time PCR, we then established the standard curve based on the results of the control DNA. Based on this standard curve, the sample Ct value was used to determine the DNA concentration of the sample. Final copy numbers of genomic DNA in the sample (copies/ml) were calculated based on the obtained sample volume and final dilution volume. High copy numbers of *Candida* DNA (9.2×10^5 copies/ml) were detected by PCR. *Aspergillus* DNA was not detected in the sample

was also found to be positive for *C. albicans*. After being treated, he had complete resolution of his symptoms.

Case 3

A 73-year-old man was referred to the Uveitis Clinic at our hospital in July 2008 because of keratic precipitates (KPs), cells in the anterior chamber, and anterior vitreous opacity in his RE that was associated with recurrent anterior uveitis. In his RE, diffuse pigmented KPs were seen (Fig. 5a). After considering both the clinical features and whole body inspections, we diagnosed this case as idiopathic uveitis. Although he was treated with topical corticosteroid and an antibiotic for 2 months, the KPs expanded (Fig. 5b). During the treatment, diffuse pigmented KPs continued to expand and then united. In addition, we also observed cells in the anterior chamber with hypopyon and dense anterior vitreous opacity. After informed consent was obtained, pars plana vitrectomy was performed in order to obtain a vitreous sample. Although fungi were not detected in a culture test, real-time PCR detected 1.8×10^3 copies/ml of the *Aspergillus* 18S rRNA gene (Table 1). Microbiological investigations performed using both culture and Gram's staining of the vitreous sample proved to be negative. A blood test for β-D-glucan and fungal antigens including *Aspergillus* were also negative. We diagnosed the patient as having *Aspergillus*-associated late postoperative endophthalmitis that was related to his 2007 cataract surgery. The patient was subsequently treated using systemic fluconazole. The medication proved to be effective in treating the infectious endophthalmitis, with the inflammation in the anterior segment of his RE completely disappearing (Fig. 5c). After treatment, *Aspergillus* DNA in his sample was below the PCR detection level.

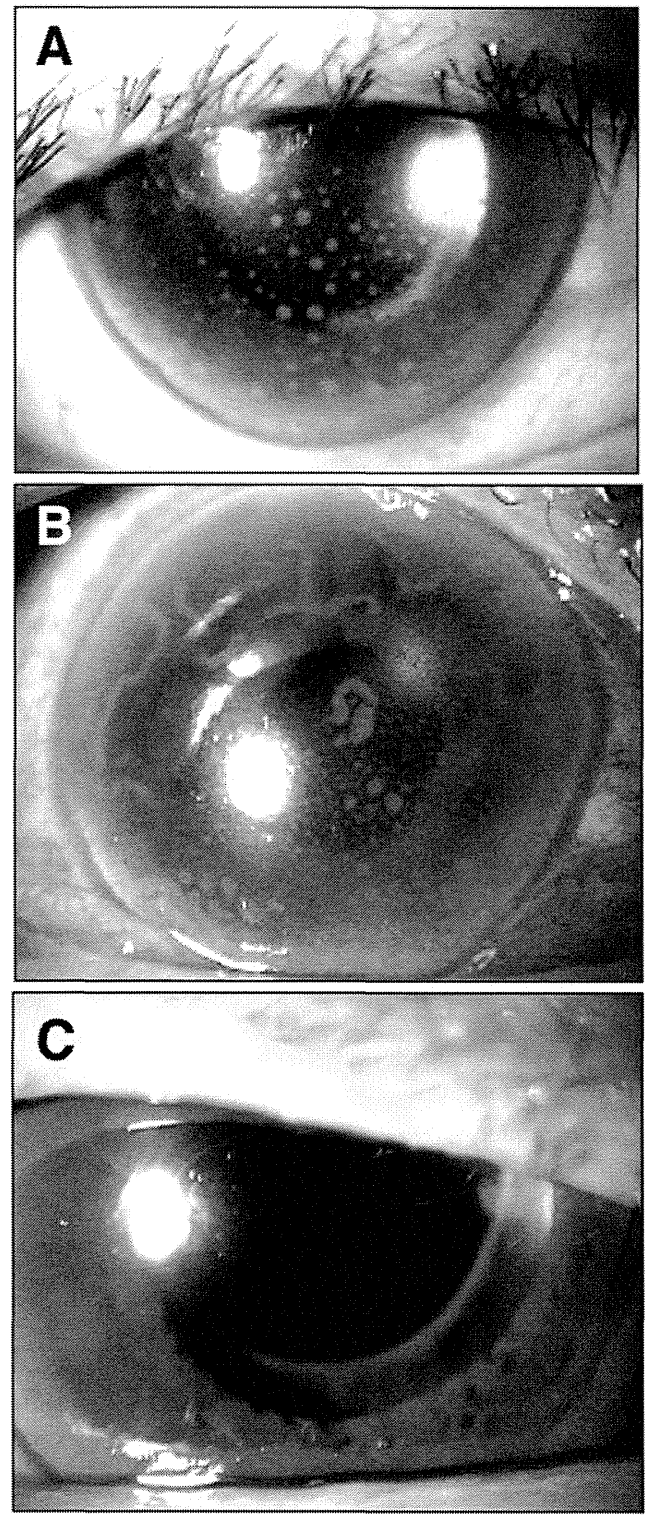

Fig. 5 PCR results for case 3. **a** Slit photograph of the right eye with an *Aspergillus* infection. Diffuse pigmented keratic precipitates (KPs) are seen. **b** The pigmented KPs are expanded and united. Like the previous case, the *Aspergillus* DNA gene (1.8×10^3 copies/ml) but not the *Candida* DNA was detected in the sample. **c** After treatment, the inflammation completely disappeared

Discussion

PCR is well suited for the detection of fungal moieties due to its specificity and applicability for use with small samples such as ocular specimens. Moreover, real-time quantitative PCR can be used to determine whether or not the fungus is related to endophthalmitis. By utilizing our broad-range real-time PCR for the 18S rRNA sequence, we were able to rapidly diagnose *Candida* or *Aspergillus* endophthalmitis in a few patients that exhibited clinical evidence of a fungal infection. While our methodology showed both positive and negative results, it was generally more helpful than waiting for culture results, as the culture tests used to detect *Candida* or *Aspergillus* are both difficult to perform and require longer amounts of time due to the slow growth rates for these species [5, 6, 13]. In addition, the specificity of our PCR examination is good enough so

that even a negative test is of benefit, as it helps to prevent making an incorrect diagnosis and administering a treatment for an infectious agent that is not present. Thus, this broad-range and real-time PCR system for ocular samples can provide a rapid diagnosis for those patients suffering from an unknown intraocular disorder such as idiopathic uveitis or endophthalmitis.

Fungal endophthalmitis is a sight-threatening disease that is most commonly caused by the *Candida* species. This disease usually accounts for a few percent of all of the cases of culture-proven endophthalmitis. The disease is normally acquired from an endogenous source that is spread by hematogenous dissemination. However, its occurrence may also be secondary to trauma, intraocular surgery, or corneal ulceration.

As confirmation of this suspected clinical disease is often difficult, there is frequently a delay in starting treatments. In the present patients, it was difficult to ascertain whether *Candida* or *Aspergillus* species were the causative agent in the intraocular inflammation. Since, in general, all of the patients were elderly and were immunocompetent, there was no focus area for the fungal infection systemically. As seen in Table 1, however, there were three exceptions. These included one case with a history of trauma (case 4), one case with a history of ocular surgery (case 3), and one case involving a normal infant (case 7), and for whom the case report details have been previously published [14].

In cases of fungal endophthalmitis in immunocompetent patients, specific additional antimycotic therapy has been shown to be effective in controlling the inflammation in the eye. In fact, all of the patients who were rapidly diagnosed by this PCR method were well controlled by the antimycotic treatment. Moreover, our PCR system was not only able to detect the conserved sequence of the fungal 18S rRNA gene, but it was also able to provide quantitative information from the ocular samples.

In recent years, PCR technology has been demonstrated to have a great potential in the detection and identification of low copy numbers of a microorganism's DNA in clinical samples [7–12, 15, 16]. It also holds great promise for being able to identify small numbers of organisms in small sample volumes, a situation that is commonly seen when trying to examine intraocular samples from patients with infectious endophthalmitis. We evaluated these PCR techniques in order to determine a reliable and effective protocol for detecting *Candida* or *Aspergillus* species DNA in ocular samples. Our specific aims were to try and significantly increase the number of intraocular samples from which a confirmed diagnosis could be made and to reduce the time it took to make a mycologic diagnosis. In many previous reports, DNAs of *Candida* and *Aspergillus* species were detected in patients with clinically suspected fungal endophthalmitis [7–10, 15–20]. For example, *Candida* species such as *C. albicans*, *C. parapsilosis*, *C. tropicalis*, *C. guilliermondii*, *C. glabrata*, and *C. krusei* have been increasingly recognized as being capable of causing fungal endophthalmitis. However, *C. albicans* has been shown to be the causative agent in the majority of cases of culture-proven endophthalmitis. Moreover, *Aspergillus* such as *A. fumigatus*, *A. flavus*, *A. nidulans*, *A. niger*, and *A. terreus* have also been reported to be the causative species in an unknown ocular infection [17–20]. To detect these fungal species, our present PCR system used paired primers and specific probes that were based upon the 18S rRNA genes of *Candida* and *Aspergillus* (see Fig. 1).

In one patient who was clinically suspected of having *Candida* endophthalmitis, our new PCR method did not detect any fungal genome in the ocular sample (case 8 in Table 1). However, it should be noted that this sample was aqueous humor and not vitreous fluid. Perhaps if a vitreous sample had been obtained, we might have detected *Candida* DNA, as *Candida* endophthalmitis often results from hematogenous dissemination. In fact, this particular patient received intravascular catheters after his initial surgery. Thus, in order to be able to make an accurate diagnosis, the type of sample that is collected may be very important.

Although there are many advantages for using our PCR assay, there is one disadvantage when attempting to diagnose fungal ocular infection. While our PCR examination was able to detect all species of *Candida* and *Aspergillus* DNA, it could not detect other fungi DNA. Recently, Vollmer et al. reported on a novel broad-range real-time PCR assay for the rapid detection of human pathogenic fungi [21]. Their assay targeted a part of the 28S large subunit rRNA (rDNA) gene. Since this PCR assay can examine *Candida* species, *Aspergillus* species, *Cryptococcus* species, among others, we are currently trying to develop a new PCR examination that uses these primers and probes for the diagnosis of fungal ocular infections, including fungal endophthalmitis.

In conclusion, utilization of the PCR assay to examine ocular samples in patients with suspected fungal endophthalmitis and idiopathic uveitis or endophthalmitis appears to be clinically useful for detecting *Candida* and *Aspergillus* DNA. Thus, broad-range PCR for the 18S rRNA sequence is a reliable tool for the diagnosis of fungal endophthalmitis and in screening for fungal infections. Moreover, because real-time PCR is an accurate method of quantitating fungal copies, real-time quantitative PCR can be used to determine whether the fungus is related to the endophthalmitis. Since the sensitivity of conventional culture techniques is not high and these cultures tend to take a long time due to their slow growth, the use of a broad-range and real-time PCR system to analyze ocular samples may be a better way to obtain a rapid diagnosis in

patients suffering from unknown intraocular infectious disorders. As early treatments are also essential for infectious endophthalmitis, this method may help to ensure that patients receive timely and optimal treatments. However, this is currently a limited research tool and not widely available for clinical labs at the present time. As a next step, we will need to work on making these tests widely available to clinical labs as oppose to only having them in research labs. In the near future, it is assumed that a comprehensive PCR system for examining fungi, bacteria, parasites, and viruses will become available, and be able to be used in the diagnosis of ocular infectious disorders.

Acknowledgements We thank Ms. Miki Katayama and Shizu Inoue for their technical assistance. We would like to also thank Drs. Hiroshi Takase and Yoshiharu Sugamoto for obtaining the samples used in this study. This work was supported by a Comprehensive Research on Disability, Health and Welfare grant, along with a Health and Labour Sciences Research Grant from the Ministry of Health, Labour and Welfare, Japan.

No financial relationships exist in the publishing of this work.

References

1. Edwards JE Jr, Foos RY, Montgomerie JZ, Guze LB (1974) Ocular manifestations of *Candida* septicemia: review of seventy-six cases of hematogenous *Candida* endophthalmitis. Medicine 53:47–75
2. Rao NA, Hidayat AA (2001) Endogenous mycotic endophthalmitis: variations in clinical and histopathologic changes in candidiasis compared with aspergillosis. Am J Ophthalmol 132:244–251
3. Klotz SA, Penn CC, Negvesky GJ, Butrus SI (2000) Fungal and parasitic infection of the eye. Clin Microbiol Rev 13:662–685
4. Walsh TJ, Anaissie EJ, Denning DW, Herbrecht R, Kontoyiannis DP, Marr KA, Morrison VA, Segal BH, Steinbach WJ, Stevens DA, van Burik JA, Wingard JR, Patterson TF, Infectious Diseases Society of America (2008) Treatment of aspergillosis; clinical practice guidelines of the Infectious Disease Society of America. Clin Infect Dis 46:327–360
5. Kunimoto DY, Das T, Sharma S, Jalali S, Majji AB, Gopinathan U, Athmanathan S, Rao TN (1999) Microbiologic spectrum and susceptibility of isolates: part I. Postoperative endophthalmitis. Endophthalmitis Research Group. Am J Ophthalmol 128:240–242
6. Puliafito CA, Baker AS, Haaf J, Foster CS (1982) Infectious endophthalmitis. Review of 36 cases. Ophthalmology 89:921–929
7. Lohmann CP, Linde HJ, Reischl U (2000) Improved detection of microorganisms by polymerase chain reaction in delayed endophthalmitis after cataract surgery. Ophthalmology 107:1047–1051
8. Ferrer C, Colom F, Frasés S, Mulet E, Abad JL, Alió JL (2001) Detection and identification of fungal pathogens by PCR and by ITS2 and 5.8S ribosomal DNA typing in ocular infections. J Clin Microbiol 39:2873–2879
9. Anand AR, Madhavan HN, Sudha NV, Therese KL (2001) Polymerase chain reaction in the diagnosis of *Aspergillus* endophthalmitis. Indian J Med Res 114:133–140
10. Jaeger EE, Carroll NM, Choudhury S, Dunlop AA, Towler HM, Matheson MM, Adamson P, Okhravi N, Lightman S (2000) Rapid detection and identification of *Candida*, *Aspergillus*, and *Fusarium* species in ocular samples using nested PCR. J Clin Microbiol 38:2902–2908
11. Sugita S, Shimizu N, Watanabe K, Katayama M, Horie S, Ogawa M, Takase H, Sugamoto Y, Mochizuki M (2011) Diagnosis of bacterial endophthalmitis by broad-range quantitative polymerase chain reaction. Br J Ophthalmol 95:345–349
12. Kami M, Fukui T, Ogawa S, Kazuyama Y, Machida U, Tanaka Y, Kanda Y, Kashima T, Yamazaki Y, Hamaki T, Mori S, Akiyama H, Mutou Y, Sakamaki H, Osumi K, Kimura S, Hirai H (2001) Use of real-time PCR on blood samples for diagnosis of invasive aspergillosis. Clin Infect Dis 33:1504–1512
13. Akler ME, Vellend H, McNeely DM, Walmsley SL, Gold WL (1995) Use of fluconazole in the treatment of *Candida* endophthalmitis. Clin Infect Dis 20:657–664
14. Ito M, Yokoi T, Sugita S, Shinohara N, Nishina S, Azuma N (2010) Endogenous *Candida* chorioretinitis in a healthy infant. Jpn J Ophthalmol 54:629–631
15. Tarai B, Gupta A, Ray P, Shivaprakash MR, Chakrabarti A (2006) Polymerase chain reaction for early diagnosis of post-operative fungal endophthalmitis. Indian J Med Res 123:671–678
16. Hidalgo JA, Alangaden GJ, Eliott D, Akins RA, Puklin J, Abrams G, Vazquez JA (2000) Fungal endophthalmitis diagnosis by detection of *Candida albicans* DNA in intraocular fluid by use of a species-specific polymerase chain reaction assay. J Infect Dis 181:1198–1201
17. Shen X, Xu G (2009) Vitrectomy for endogenous fungal endophthalmitis. Ocul Immunol Inflamm 17:148–152
18. Moinfar N, Smiddy WE, Miller D, Miller D, Herschel K (2007) Posttraumatic *Aspergillus terreus* endophthalmitis masquerading as dispersed lens fragments. J Cataract Refract Surg 33:739–740
19. Kramer M, Kramer MR, Blau H, Bishara J, Axer-Siegel R, Weinberger D (2006) Intravitreal voriconazole for the treatment of endogenous *Aspergillus* endophthalmitis. Ophthalmology 113:1184–1186
20. Kalina PH, Campbell RJ (1991) *Aspergillus terreus* endophthalmitis in a patient with chronic lymphocytic leukemia. Arch Ophthalmol 109:102–103
21. Vollmer T, Störmer M, Kleesiek K, Dreier J (2008) Evaluation of novel broad-range real-time PCR assay for rapid detection of human pathogenic fungi in various clinical specimens. J Clin Microbiol 46:1919–1926

Dysregulated microRNAs affect pathways and targets of biologic relevance in nasal-type natural killer/T-cell lymphoma

Siok-Bian Ng,[1] *Junli Yan,[2] *Gaofeng Huang,[3] Viknesvaran Selvarajan,[1] Jim Liang-Seah Tay,[4] Baohong Lin,[3] Chonglei Bi,[2] Joy Tan,[4] Yok-Lam Kwong,[5] Norio Shimizu,[6] Katsuyuki Aozasa,[7] and Wee-Joo Chng[2-4]

[1]Department of Pathology, National University Health System, Singapore; [2]Cancer Science Institute of Singapore, National University of Singapore, Singapore; [3]Department of Haematology-Oncology, National University Cancer Institute of Singapore, National University Health System, Singapore; [4]Department of Medicine, Yong Loo Lin School of Medicine, National University of Singapore, Singapore; [5]Division of Haematology/Oncology and Bone Marrow Transplantation, Queen Mary Hospital, Hong Kong; [6]Department of Virology, Tokyo Medical and Dental University, Tokyo, Japan; and [7]Department of Pathology, Osaka University Graduate School of Medicine, Osaka, Japan

We performed a comprehensive genome-wide miRNA expression profiling of extranodal nasal-type natural killer/T-cell lymphoma (NKTL) using formalin-fixed paraffin-embedded tissue (n = 30) and NK cell lines (n = 6) compared with normal NK cells, with the objective of understanding the pathogenetic role of miRNA deregulation in NKTL. Compared with normal NK cells, differentially expressed miRNAs in NKTL are predominantly down-regulated. Re-expression of down-regulated miRNAs, such as miR-101, miR-26a, miR26b, miR-28-5, and miR-363, reduced the growth of the NK cell line and modulated the expression of their predicted target genes, suggesting the potential functional role of the deregulated miRNAs in the oncogenesis of NKTL. Taken together, the predicted targets whose expression is inversely correlated with the expression of deregulated miRNA in NKTL are significantly enriched for genes involved in cell cycle-related, p53, and MAPK signaling pathways. We also performed immunohistochemical validation for selected target proteins and found overexpression of MUM1, BLIMP1, and STMN1 in NKTL, and notably, a corresponding increase in MYC expression. Because MYC is known to cause repression of miRNA expression, it is possible that MYC activation in NKTL may contribute to the suppression of the miRNAs regulating MUM1, BLIMP1, and STMN1. (*Blood*. 2011;118(18):4919-4929)

Introduction

Extranodal nasal-type natural killer/T-cell lymphoma (NKTL) is an aggressive lymphoma with a strong association with EBV. The pathogenesis of this tumor is poorly understood, but in recent years gene expression profiling (GEP) studies have demonstrated the pathogenetic role of several oncogenic pathways in NKTL, such as AKT, STAT3, NF-κB, Notch-1, and Aurora kinase A.[1,2] We recently performed a genome-wide GEP using formalin-fixed paraffin-embedded (FFPE) tissue and, in addition to NF-κB, we also identified deregulation of c-Myc and p53 pathways, and overexpression of survivin in NKTL.[3]

MicroRNAs (miRNAs) are short, noncoding RNAs that post-transcriptionally regulate the expression of multiple mRNAs. To date, > 1000 human miRNA precursor sequences have been identified and deposited in miRBase.[4] miRNAs play a key role in the control of normal biologic processes, including hematopoiesis, and have been implicated in the development of human cancer.[5,6] In lymphoid malignancies, miR-155 is overexpressed in Hodgkin lymphoma and non-Hodgkin lymphoma, and dysregulation of miR-16-1 control of cyclinD1 has been reported in mantle cell lymphoma. Yamanaka et al performed northern analysis on NKTL using a limited number of probe sets and found overexpression of miR-155 and miR-21, which results in the activation of AKT signaling.[7] Furthermore, quantification of miRNAs can have potential diagnostic and prognostic utility in lymphoma.[5,6,8] miRNA expression profiling (MEP) has been increasingly used in cancer research; and in recent years, it has been possible to obtain meaningful and reproducible profiles using FFPE tissue.[9] To the best of our knowledge, there have been no reports of genome-wide MEP on NKTL in the published literature.

In this study, we performed the first miRNA expression profiling on a series of NKTL using FFPE tissues in relation to normal NK cells and NK tumor cell lines, with the main objective of understanding the pathogenic role and mechanisms of miRNA dysregulation in NKTL. We also performed a combined analysis of the miRNA profiles, and the gene expression profiles obtained in our previous study using bioinformatics target prediction with subsequent functional validation to identify essential target genes and signaling pathways that are deregulated by miRNA in NKTL.

Methods

Case selection, cell lines, and control tissues

Patients with a diagnosis of NKTL were identified from the archives of the Department of Pathology, National University Hospital, from 1990 to 2010 and classified according to the 2008 WHO lymphoma classification. Cases with no additional tissue available for immunohistochemical or genetic analysis were excluded. A total of 38 cases of NKTL were selected, of which 33 cases were used for tissue microarray construction and 9 cases were subjected to GEP in our previous study.[3] According to the WHO

Submitted July 3, 2011; accepted September 3, 2011. Prepublished online as *Blood* First Edition paper, September 14, 2011; DOI 10.1182/blood-2011-07-364224.

*J.Y. and G.H. contributed equally to this study.

The online version of this article contains a data supplement.

The publication costs of this article were defrayed in part by page charge payment. Therefore, and solely to indicate this fact, this article is hereby marked "advertisement" in accordance with 18 USC section 1734.

criteria, all cases expressed CD3, cytotoxic markers (granzyme B and/or TIA-1), and EBER. Immunoreactivity for CD56, CD8, and CD4 was present in 66% (25 cases), 13% (5 cases), and 5% (2 cases), respectively. The clinical and immunophenotypic data of the cases are summarized in supplemental Table 1 (available on the *Blood* Web site; see the Supplemental Materials link at the top of the online article).

Thirty cases of NKTL with adequate FFPE tissue and good-quality RNA were selected for miRNA profiling. The study also included 6 NK cell lines (KHYG-1, NK-92, HANK-1, SNT-8, SNK-6, and NK-YS). In addition, 3 paired samples of normal NK cells (unstimulated and stimulated) as well as 2 cases each of normal skin, intestinal, nasal, and lymph node FFPE tissue were also included as control tissue. The study is approved by the Domain Specific Review Board of the National Healthcare Group, Singapore.

NK cell lines and cultures

The NK-tumor cell lines used in this study included NK-92 (ATCC), KHYG-1 (Japanese Collection of Research Bioresources), HANK-1 (gift from Dr Yoshitoyo Kagami), SNK-6, SNT-8 (gift from Dr Norio Shimizu), and NK-YS (gift from Dr YL Kwong). The culture conditions and phenotypic and genotypic characteristics of the NK cell lines, which are well characterized in previous studies,[10,11] are summarized in supplemental Table 2. Although 2 of these cells lines are derived from Aggressive Natural Killer-cell leukemia (KHYG and NK-92), only very few miRNAs (24 of 723 miRNAs on chip, 3%) have 2-fold or more difference in expression between these and the other NK/T lymphoma cell lines. They were therefore grouped together as NKTL cell lines for comparison of miRNA expression against tumor samples from patients.

Isolation of normal NK cells from peripheral blood

Highly purified (90%-99%) untouched normal human NK cells were isolated from whole blood samples obtained from healthy donors and buffy coat packs of whole blood samples from the Blood Donation Center, National University Hospital, using the NK cell isolation kit (Miltenyi Biotec) as previously described.[3] The isolated NK cells were subsequently stimulated by culturing in the presence of human recombinant IL-2 (Miltenyi Biotec). Cell block preparations of normal NK cells were prepared as previously described.[3]

RNA extraction from FFPE, NK cell lines, and normal NK cells

Total RNA from NKTL FFPE tissues and FFPE normal tissue controls was isolated using RecoverAll Total Nucleic Acid Isolation (Applied Biosystems) according to the manufacturer's instructions. All the sections were deparaffinized with xylene, subjected to proteinase K digestion, and RNA extracted as per the manufacturer's protocol.

Total RNA was extracted from freshly isolated cells from NK cell lines and normal NK cell samples obtained from healthy donors using miRNeasy mini kit (QIAGEN) protocol with DNaseI treatment included. The concentration and purity of the total RNA extracted were measured using the NanoDrop ND Version 3.0 spectrophotometer (NanoDrop Technologies). RNA quality was assessed with the Agilent 2100 Bioanalyzer (Agilent Technologies) and the RNA 6000 LabChip kit (Agilent Technologies).

miRNA profiling and analysis

miRNA expression was profiled using Agilent human miRNA Microarray Version 2 (Agilent Technologies). Each array contained 60-mer probes representing 723 human and 76 human viral miRNAs from the miRBase Version 10.1. The array experiment was carried out using Agilent miRNA system protocol Version 2.0. Briefly, each RNA sample was labeled with Cyanine3-pCp and hybridized to the Agilent human miRNA microarray using the miRNA Complete Labeling and Hyb Kit (Agilent p/n 5190-0456). The slide was washed using Gene Expression Wash Buffer Kit (Agilent p/n 5188-5327) and then scanned using an Agilent DNA microarray scanner. The raw miRNA expression data were extracted from the scanned image using Agilent Feature Extraction Version 10 software. The raw expression values of miRNA were normalized and analyzed using R Version 2.11.0 and Bioconductor Version 2.8. The microarray data are deposited on the Gene Expression Omnibus (accession number GSE31377).

Transfection of synthetic miRNAs and anti-miRNA inhibitors

miRNA mimics, which are chemically synthesized double-stranded RNA molecules, were designed to mimic endogenous mature miRNAs. They enable detailed study of miRNA biologic effects via gain-of-function experiments.[12-14] Cells were transfected with miRNA mimics (Dharmacon RNA Technologies) and anti-miRNA inhibitors (Ambion) at a final concentration of 50nM using DhamarFECT (Dharmacon RNA Technologies) according to the manufacturer's instructions. The control miRNA mimic used was a mimic based on *Caenorhabditis elegans* miRNA (cel-miR-67). The anti-miRNA inhibitor negative control #1 purchased from Ambion is an RNA oligonucleotide designed to serve as a negative control for experiments involving anti-miRNA inhibitors. Total RNA and protein were collected for assay 2 days after transfection.

Cell growth assay

To generate cell growth curve, cells were harvested and counted at 24-hour intervals. The counting results were validated using the CellTiter 96 AQueous Non-Radioactive Cell Proliferation Assay (Promega) by a linear relationship ($r^2 = 0.99$) between the number of cells and absorbance at 490 nm from each well.

Re-expression of miRNAs using lentivectors

Expression of miRNA precursors were driven by CMV promoters in a HIV-based lentiviral vector purchased from Systems Biosciences. The construct consists of the native stem loop structure of miRNA and 200 to 400 bp of upstream and downstream flanking genomic sequence cloned into the pMIRNA1-plasmid. Packaging of the miRNA constructs in pseudoviral particles was performed using the third-generation packaging system. NK-YS cells were infected with the lentivirus with an efficiency of ~ 95% as determined by green fluorescent protein measurement by flow cytometry. Empty vector lentivirus was used as a control for the experiments.

Real-time RT-PCR quantification of miRNAs

Total RNAs, including small RNAs, were purified by miRNeasy Mini Kit (QIAGEN). cDNAs were synthesized from total RNA using TaqMan MicroRNA Reverse Transcription Kit with gene-specific primers. Reverse transcription reactions (for final quantity or concentrations) contained 10-ng RNA samples, 0.67μM of dNTP, 1× RT primer, 1× RT buffer, 3.8 U of RNAse inhibitor, and 50 U of reverse transcriptase. The 15-μL reactions were incubated for 30 minutes at 16°C, 30 minutes at 42°C, 5 minutes at 85°C, and then held at 4°C. Real-time RT-PCR quantification of miRNA expression was carried out using TaqManR MicroRNA Assays Kit (Applied Biosystems) according to the manufacturer's protocol. The 20-μL PCR included 1.33 μL RT product, 1× PCR Master mix, and 1× TaqMan-primers mix (Applied Biosystems). Reactions were incubated in a 96-well plate at 95°C for 10 minutes, followed by 40 cycles of 95°C for 15 seconds and 60°C for 1 minute. The threshold cycle (C_t) was determined using default threshold settings. All experiments were done in triplicates. The U6 snRNA was used as a control to normalize miRNA input in the real-time RT-PCR assay.

Real-time RT-PCR quantification of mRNAs

cDNAs from total RNA were obtained by the SuperScriptR III Reverse Transcriptase (Invitrogen) according to the manufacturer's instructions. SYBR PCR Master Mix (Applied Biosystems) was used for quantitative PCR as recommended by the manufacturer. GAPDH was used as a control to normalize mRNA input. All experiments were done in triplicates.

Luciferase reporter assay

A PCR-amplified fragment that contains 2 predicted miR-101 binding sites at the 3′-UTR of STMN1 was cloned into a dual-luciferase expression vector pmirGLO (Promega) to create the STMN1 reporter constructs. The seed and surrounding sequences at binding site #1 (position 278-292 of

Table 1. Deregulated miRNA in NKTL and NK cell lines compared with normal NK cells

	Cell lines versus normal		NKTL versus normal				
miRNA	q-value	Fold change	q-value	Fold change	Chromosome location	Genomic position	Target genes
hsa-miR-342–5p	0.00047	0.17804	0.00000	0.17231	14	099645783-099645765	POFUT1
hsa-miR-26b	0.00049	0.05876	0.00000	0.02942	2	218975644-218975625	BCL2, IGF1, SETD7, FOXP2, CAPRIN1, PSD3, HOXA5, KPNA2, E2F7, ENPEP, EZH2, HMGA1, NAMPT, PIM1, SC4MOL, ACVR1C, AGPAT5, ASCC3, CKS2, CTTNBP2NL, DCDC2, IARS, KIF18A, LARP1, MTM1, NFE2L3, NUP50, SLC7A11
hsa-miR-363	0.00049	0.05325	0.00000	0.06310	X	133131078-133131095	BCL2, IGF1, SETD7, FOXP2, PSD3, ATP2A2, BCAT2, DOCK9, SMAD6, ADCY3, ASB7, CHCHD10, FMN2, NFIB, RAB23, RGL1, SLC7A11, YIPF4
hsa-miR-150	0.00049	0.00483	0.00000	0.01099	19	054695901-054695916	MYB, ELK1, CTH, ENSA
hsa-miR-28–5p	0.00049	0.17303	0.00000	0.14000	3	189889297-189889278	IGF1, SETD7, CAPRIN1, HTRA2, MAD2L1, TLN2
hsa-miR-152	0.00049	0.28067	0.00000	0.27612	17	043469539-043469553	E2F7, ANK2, ATP2A2, B4GALT2, BBC3, CEP55, DPP3, EMP1, HMGB3, IGF1, KLC2
hsa-miR-361–3p	0.00049	0.23188	0.00000	0.19701	X	085045302-085045320	CD3EAP, OSR2
hsa-miR-22*	0.00049	0.32882	0.00000	0.34642	17	001563996-001564012	No predicted targets
hsa-miR-340	0.00049	0.26426	0.00000	0.29925	5	179374967-179374984	AGPAT5, AHR, CDON, CIT, DEPDC1B, E2F7, FHL2, GK, HECW2, IGF1, ING3, MYO1C, NUPL1, PHLDA1, SLC7A11, TIAM1
hsa-miR-598	0.00049	0.49291	0.00000	0.48708	8	010930141-010930158	No predicted targets
hsa-miR-181a-2*	0.00049	0.23242	0.00000	0.22641	9	126494639-126494623	No predicted targets
hsa-miR-132	0.00050	0.45398	0.00000	0.42973	17	001899973-001899987	HBEGF, BRI3, HN1, TLN2, VDAC2, ADCY3, AHCY, AZIN1, CAPRIN1, FKBP2, NFIB, PPM1G, SCN2A, TRIB1, TTK
hsa-miR-194	0.00050	0.32209	0.00024	0.32691	1	218358171-218358185	HBEGF, TLN2, CTAGE5, LPHN2, PRR7, VDAC2
hsa-miR-768–3p	0.00050	0.13168	0.00000	0.08066	16	070349814-070349832	AHR, CENPE, HOXA4
hsa-miR-873	0.00050	0.22803	0.00000	0.22284	9	028878923-028878939	FOXK2, MPDU1, TLN2
hsa-miR-338–3p	0.00052	0.13277	0.00001	0.15864	17	076714282-076714301	FKBP1A, ARPC1B
hsa-miR-215	0.00053	0.44650	0.00119	0.45644	1	218357881-218357900	DYRK3, LPAR4, TRIP13
hsa-miR-186	0.00054	0.26956	0.00000	0.14583	1	071305952-071305971	CDC42, BTF3, PPM1G, SMAD6, ACSL4, BCAT1, BMP2K, EIF2S2, ENPEP, PRDM1, PSD3, PSMD11, PSPH, RGS22, VEGFA, ZCCHC5
hsa-miR-140–3p	0.00054	0.27234	0.00000	0.16194	16	068524566-068524552	FOXK2, UBE2C
hsa-miR-140–5p	0.00054	0.30678	0.00000	0.13482	16	068524528-068524508	ARHGAP19, CASP3, ST5, TTK
hsa-miR-374b	0.00055	0.32813	0.00000	0.13347	X	073355147-073355164	TFDP1, CCNE2, EIF2S2, EIF4G1, ENSA, GNB2, HOXA11, HSPA4, HTRA2, LARP1, NFIB, SMAD6
hsa-miR-26a	0.00056	0.14699	0.00048	0.23283	12	056504708-056504721	BCL2, IGF1, SETD7, PSD3, EZH2, HOXA5, KPNA2, E2F7, ENPEP, HMGA1, NAMPT, PIM1, SC4MOL, ASCC3, CKS2, CTTNBP2NL, DCDC2, IARS, KIF18A, LARP1, MTM1, NFE2L3, NUP50, SLC7A11
hsa-let-7g	0.00057	0.21467	0.00001	0.10030	3	052277392-052277411	ACVR1C, AP1S1, CASP3, CDC25A, COL15A1, CYP19A1, DPP3, EZH2, FAM118A, POLR3D, SCD, TARBP2, TTLL4, ATP2A2, BCAP29, BCAT1, CCNF, CD86, DUSP4, HMGA1, RGS16, SOCS1, THRSP, ZCCHC5
hsa-miR-342–3p	0.00057	0.14972	0.00000	0.07856	14	099645827-099645812	ENSA, SLC35F2, TIAM1
hsa-miR-101	0.00057	0.33272	0.00000	0.09962	1	065296713-065296731	STMN1, BCL2, IGF1, PSD3, EZH2, EMP1, ING3, PANK3, PHLDA1, TRIB1, ACCN2, ASCC3, DDIT4, HNRNPAB, LMNB1, POMP, SCN2A, SELI
hsa-miR-192	0.00060	0.33056	0.00044	0.32841	11	064415251-064415268	DYRK3, LPAR4, TRIP13
hsa-miR-374a	0.00065	0.29720	0.00000	0.09324	X	073423885-073423905	EIF2S2, ENSA, GK, GNB2, HOXA11, HSPA4, LARP1, NFIB, SMAD6, TFDP1
hsa-miR-876–5p	0.00070	0.43160	0.00004	0.39927	9	028853673-028853691	EME1, FOXM1, DNAJC12, NTRK2, PHLDA1, TFAP2A, ZCCHC5

Table 1. Deregulated miRNA in NKTL and NK cell lines compared with normal NK cells (continued)

	Cell lines versus normal		NKTL versus normal				
miRNA	q-value	Fold change	q-value	Fold change	Chromosome location	Genomic posiltion	Target genes
hsa-miR-22	0.00076	0.19107	0.00000	0.19752	17	001563958-001563975	BATF3, DDIT4, HOXA4, IPO7, MTHFD2, RFXANK, APBB2, NET1, PPM1G, TIAM1
hsa-miR-10a	0.00111	0.42780	0.00008	0.36971	17	044012265-044012284	BCL6, SOBP, STK24, TIAM1, ZNF367
hsa-miR-590–5p	0.00168	0.45785	0.00000	0.17107	7	073243500-073243479	ING3, NFIB, RBPJ, TIAM1, ZNF367
hsa-miR-30b	0.00258	0.26088	0.00000	0.09993	8	135881995-135882010	ADAM22, DDIT4, NFIB, PPARGC1B, SCN2A, SLC41A2, ASCC3, CCNE2, CELSR3, FGD6, PRDM1, RHEBL1, SCN8A, SMARCD2, SOCS1, AVEN, AZIN1, BCL2, DEPDC4, FRMD6, HOXA11, IL2RA, IRF4, ITSN1, MTA1, PRICKLE1, RGL1, SETD7, STXBP1, SUPT3H, TFDP1
hsa-miR-181c	0.00324	0.40588	0.00000	0.24845	19	013846560-013846542	FKBP1A, NR6A1, CTTNBP2NL, DDIT4, E2F7, HOXA11, NR4A3, APOO, ATP2A2, CDON, FAM3C, IPPK, ITSN1, MAP1A, MINA, NLN, PDIA6, PHLDA1, PRDX3, SCD, SLC25A37
hsa-miR-142–5p	0.00404	0.34288	0.00000	0.01692	17	053763643-053763660	SRI, AHR, HN1, PPM1G, RBBP8, RNH1, SLC41A2
hsa-let-7a	0.00602	0.45269	0.00420	0.37315	11	121522486-121522504	ACVR1C, AP1S1, CASP3, CDC25A, CYP19A1, DPP3, EZH2, SCD, TARBP2, ATP2A2, BCAP29, BCAT1, BRF2, CCNF, COL15A1, DUSP4, FAM118A, HOXB4, POLR3D, RGS16, SOCS1, THRSP, TRIB1, TTLL4, ZCCHC5
hsa-miR-155	0.00690	11.45284	0.00119	2.16728	21	025868188-025868172	BNC2, SGK3, TLE4, TSHZ3, EIF2C4, FGF7, GPM6B, KLRC3, LHX9, MYLK, PCDH9, PDLIM5, RAB34, RREB1, SOX11, ZNF618
hsa-let-7c	0.01070	0.27938	0.00160	0.41876	21	016834050-016834032	ACVR1C, CASP3, CDC25A, CYP19A1, DPP3, EZH2, SCD, TARBP2, TTLL4, AP1S1, ATP2A2, BCAT1, BRF2, CCNF, COL15A1, DUSP4, FAM118A, HOXB4, POLR3D, RGS16, SOCS1, THRSP, TRIB1
hsa-miR-378	0.01145	2.53182	0.00059	4.08760	5	149092643-149092631	GPM6B, IGF1R, WDR37
hsa-miR-181a	0.01665	0.38679	0.00000	0.16954	1	197094860-197094873	FKBP1A, NR6A1, CTTNBP2NL, DDIT4, E2F7, HOXA11, NR4A3, APOO, ATP2A2, CDON, FAM3C, IPPK, ITSN1, MAP1A, MINA, NLN, PDIA6, PHLDA1, PLAU, PRDX3, SCD, SLC25A37
hsa-miR-142–3p	0.01796	0.45692	0.00000	0.01686	17	053763605-053763626	TFG, FKBP1A, GNB2, ATP2A2
hsa-miR-15a	0.04502	0.49695	0.00000	0.13992	13	049521304-049521323	CCNE1, CDCA4, CHEK1, MYB, WEE1, CDC25A, KIF23, LPHN2, PDIA6, PPAP2A, SMARCD2, STXBP1, TARBP2, ACSL4, ANKRD13B, BCL2, BTF3, CDC42, E2F7, FKBP1A, FSD1, IARS, LIPE, OTX1, PANK1, PHF19, PIM1, PPIF, PPIL1, PTPN3, SELI, SMYD5, ZCCHC5

3′-UTR, ATGGCTAGTACTGTA) and site #2 (position 437-448, CACAGTGCTGTT) within this construct were separately mutated to CTGGCTAATACGGTA and CGCAGCGCTCTC, respectively, using a Quick-change II site-directed mutagenesis kit (Agilent/Stratagene). The reporter construct containing full-length PRDM1 3′-UTR, the miR-101 and miR-186 precursor expression vectors, and their corresponding control plasmids were purchased from GeneCopoeia, System Biosciences, and Cell Biolabs, respectively. HEK-293T cells were cotransfected, in triplicate wells, with STMN1 reporter construct and miR-101 precursor expression vector at a ratio of 1:6 using Lipofectamine (Invitrogen) for 48 hours. PRDM1 reporter construct and miR-186 precursor vector were similarly transfected at a ratio of 1:200 for 72 hours before harvest. Firefly and Renilla luciferase activities of cell lysates were determined by a dual-luciferase reporter assay system (Promega). The ratio of firefly to Renilla luminescence of cells ectopically expressing miRNAs was compared with that of cells transfected with control miRNA precursor plasmid. miRNA overexpression was confirmed by real-time PCR using TaqMan probes specific to respective miRNAs. Results are presented as averages of 3 independent experiments.

IHC

Immunohistochemistry (IHC) was performed for MUM1, BLIMP1, and STMN1on 4-μm sections from the TMA blocks of NKTL cases. For those cases that were not included in the TMA, 4-μm sections were cut from whole paraffin blocks (5 cases). IHC was also performed on cell blocks of normal NK cells for comparison (see supplemental Table 3 for more details). Appropriate positive tissue controls were used. The immunohistochemical expression for all the antibodies was scored as a percentage of the total tumor cell population per 1-mm core diameter (× 400) by one of the authors (S.-B.N.), as previously described.[3] For MUM1and BLIMP1 antibodies, positive expression was defined as nuclear staining in 20% or more of the tumor population. For STMN1, positive

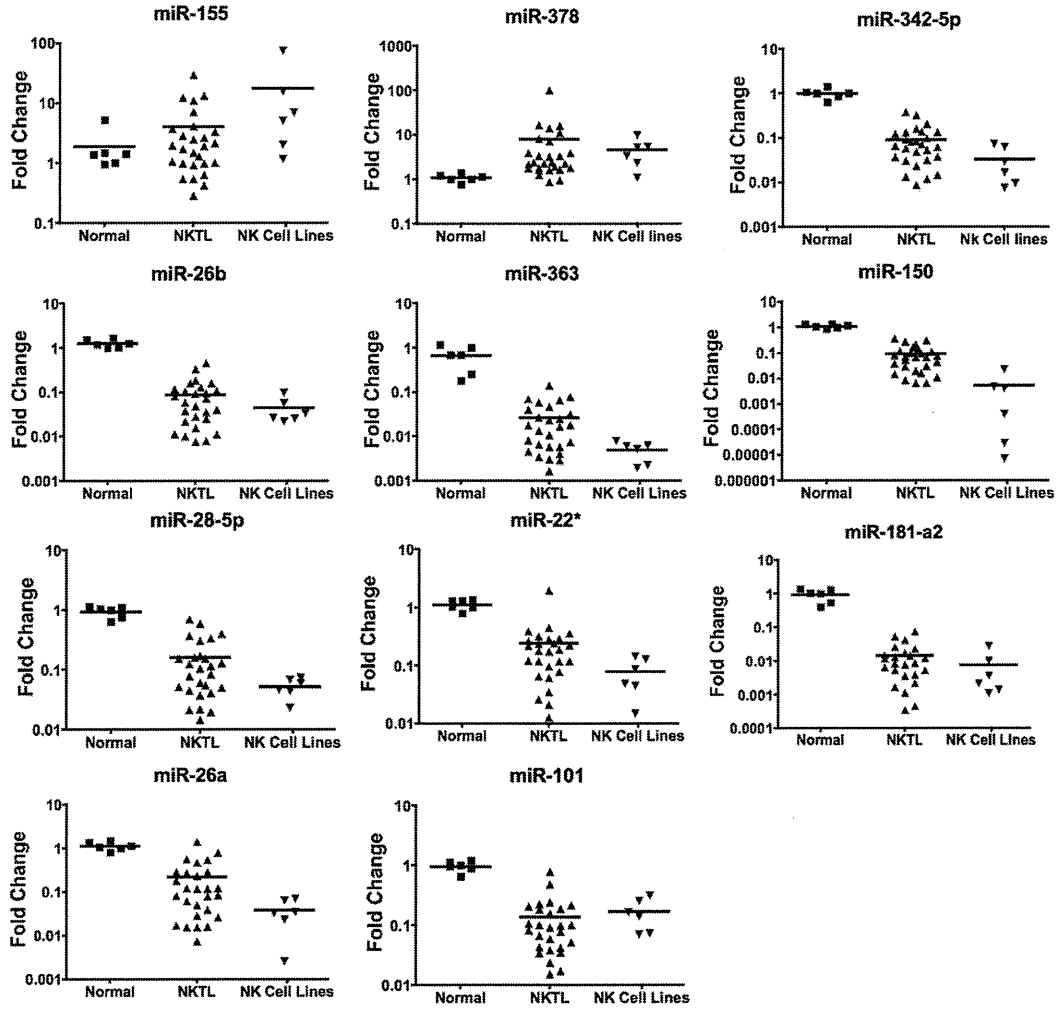

Figure 1. Quantitative RT-PCR validation of miRNA expression profiling data. Eleven miRNAs that were deregulated in NKTL were selected for validation by quantitative RT-PCR. In every case, miRNAs down-regulated in NKTL compared with normal NK cells were also found to be down-regulated by quantitative RT-PCR. Similar observations were made for up-regulated miRNAs. All comparisons are statistically significant ($P < .05$).

expression was defined as cytoplasmic and/or nuclear staining in 20% or more of the tumor population.

Results

miRNA dysregulation in NKTL

We compared the miRNA expression of NKTL FFPE samples (n = 30) with that of normal NK cells and the respective normal FFPE tissue controls from nasal, skin and soft tissue, intestinal tract, and lymph node, as well as that of NK cell lines with normal NK cells (supplemental Tables 4 and 5). Among the miRNAs showing at least 2-fold and statistically significant difference ($P < .05$) in expression, 2 were found to be up-regulated and 39 were down-regulated in both NK cell lines and FFPE NKTL samples compared with normal NK cells (Table 1). miR-342–5p, miR-26b, miR-363, miR-150, and miR28–5p are the top 5 down-regulated miRNAs, whereas miR-155 and miR-378 are up-regulated in both NK cell lines and FFPE NKTLs.

We performed quantitative PCR validation of 11 selected miRNAs, including the top 5 down-regulated miRNAs, 2 up-regulated miRNAs, and a few interesting miRNAs, which may be involved in tumor oncogenesis. On the whole, quantitative PCR results were consistent with MEP data showing overexpression of miR-155 and miR-378 and underexpression of miR-342–5p, miR-26b, miR-363, miR-150 and miR28–5p, miR-22*, miR-181a-2*, miR-26a and miR-101 in NK cell lines and NKTL FFPE samples compared with normal NK cells (Figure 1).

The validity of the MEP platform and results was further verified by comparing the miRNA expressed in our normal and stimulated NK cells with that detected by sequencing methods.[15] There is substantial overlap between our data list and the list generated by sequencing method (supplemental Figure 1).

Functional relevance of dysregulated miRNAs in NKTL

To assess the relevance of the dysregulated miRNAs to the biology of NKTL, we incubated the NKYS cell line with miRNA mimics for down-regulated miRNAs, including miR-101, miR-363, miR-28–5p, miR-26a, miR-26b, miR-342–5p, and miR-181a-2*, and miRNA inhibitor for one of the overexpressed miRNAs, miR-155. The use of miR-101, miR-363, miR-28–5p, miR-26a, and miR-26b mimics substantially reduced growth of NK-YS cells (Figure 2). This suggests that these miRNAs could play a potential role in the growth and proliferation of NKTL.

Next, we identified high-probability predicted target genes of these deregulated miRNAs by intersecting targets predicted by 6 algorithms,

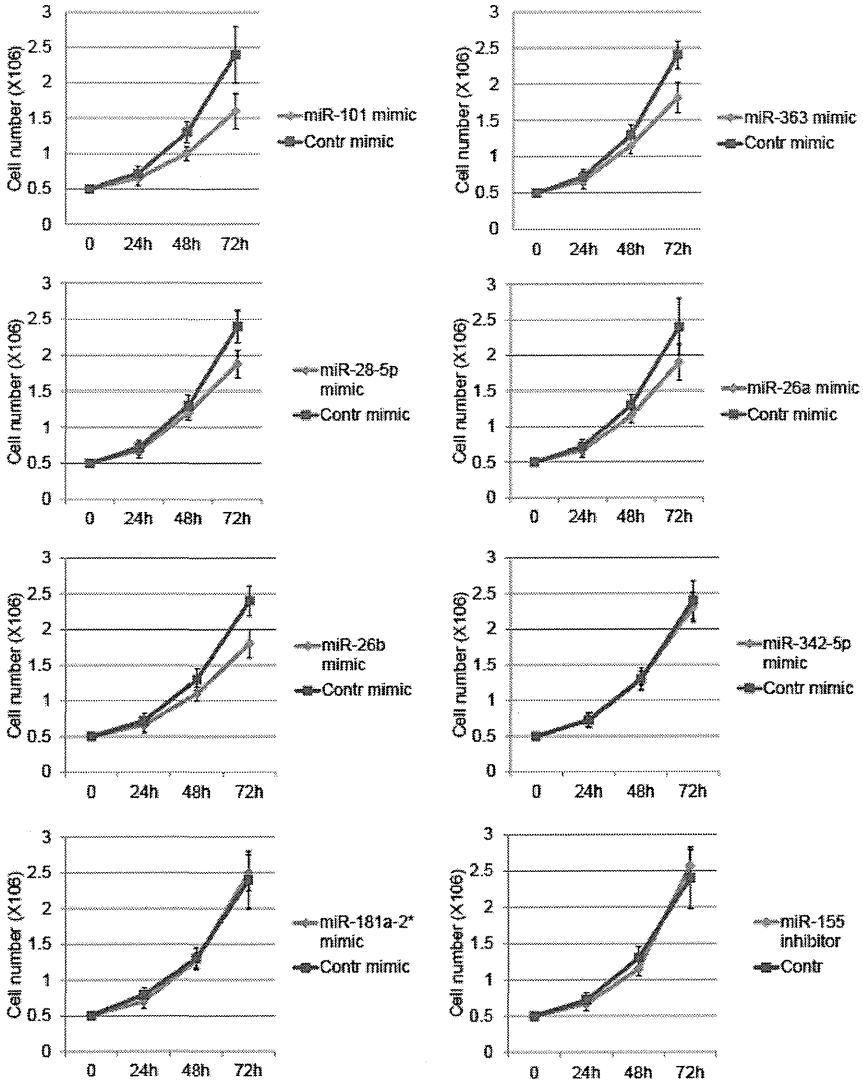

Figure 2. Effect of deregulated miRNAs on growth of NKTL cells. Growth curves of NK-YS cells transfected with synthetic miRNAs and anti-miRNA inhibitors. Cell number was counted at the indicated time points after transfections. Counting results were validated by Cell-Titer 96 Cell Proliferation Assay. Error bars represent SD; n = 3.

including mirBase (http://microrna.sanger.ac.uk), targetScan (http://www.targetscan.org), miRanda (http://www.microrna.org), tarBase (http://diana.cslab.ece.ntua.gr/tarbase), mirtarget2 (http://mirdb.org/miRDB), and pictar (http://pictar.mdc-berlin.de; Table 1). We further assessed the expression of the target genes in those samples that also have GEP done and further narrowed down the relevant target genes to those whose expression is inversely correlated with the expression of the deregulated miRNAs. We selected a number of target genes of the 3 miRNAs (miR-101, miR-26a, and miR-26b), which were shown to alter the growth of NK-YS for further validation. We used lentiviral vectors as an alternate method to express miR-101, miR-26a, and miR-26b in NK-YS. This resulted in a significant increase in the expression of these miRNAs and a corresponding decrease in the expression of *STMN1* (Figure 3A), one of the target genes of miR-101, and *BCL2*, a target gene shared by miR-101, miR-26a, and miR-26b (Figure 3C). On the other hand, *IGF1* is only down-regulated on mir-101 expression but not miR-26a or miR-26b expression, although it is also predicted to be targets of all 3 miRNAs (Figure 3C). This inconsistency may be explained by the known discrepancies between predicted target and actual targets. We therefore proceeded to validate several miRNAs and their predicted targets, which may be of relevance in NKTL. In the 3′-UTR of *STMN1*, there are 2 predicted binding sites of miR-101. To confirm that miR-101 binds to 3′-UTR of *STMN1* and affects its expression, and to clarify which of these binding sites are the most important, we performed luciferase assay with different *STMN1* 3′-UTR constructs; no mutation, first binding sequence mutated (MUT1) or second binding sequence mutated (MUT2) (supplemental Figure 2). Our results showed that the reporter with the fragment of 3′-UTR of *STMN1* that contains the 2 seed sequences reduced luciferase activity. The MUT1 reporter construct (with the first seed sequence mutated) showed similar level of luciferase activity as the wild-type reporter construct, whereas the MUT2 reporter construct (with the second seed sequence mutated) demonstrated a restoration to the same level as the empty control reporter. This suggests that the second seed sequence is the critical binding site for miR-101.

Next, we validated the relationship between miR-30b (underexpressed in NKTL) and *PRDM1* (gene encoding BLIMP1), which has been shown to be important for NK cell maturation and may therefore be of biologic relevance to NKTL. The use of miR-30b mimic in NKYS leads to repression of *PRDM1* mRNA expression. The effect of miR-30b on *PRDM1* expression is confirmed on luciferase reporter assay when expression of miR-30b precursor inhibited *PRDM1* expression (Figure 3B). These results provide further evidence that deregulation of miRNA is of functional and biologic relevance in NKTL.